2011-01-01

A Third-Order Non-Oscillatory Finite-Volume Transport Scheme For Atmospheric Modeling

Kiran Kumar Katta
University of Texas at El Paso, kattakiran@gmail.com

A THIRD-ORDER NON-OSCILLATORY FINITE-VOLUME TRANSPORT SCHEME FOR ATMOSPHERIC MODELING

KIRAN KUMAR KATTA

Program in Computational Science

APPROVED:

Vinod Kumar, Ph.D., Chair

Ramachandran D. Nair, Ph.D.

Andrzej Pownuk, Ph.D.

Patricia D. Witherspoon, Ph.D.
Dean of the Graduate School

A THIRD-ORDER NON-OSCILLATORY TRANSPORT SCHEME FOR ATMOSPHERIC MODELING

by

KIRAN KUMAR KATTA, B.S., M.S.

THESIS

Presented to the Faculty of the Graduate School of

The University of Texas at El Paso

in Partial Fulfillment

of the Requirements

for the Degree of

MASTER OF SCIENCE

Program in Computational Science

THE UNIVERSITY OF TEXAS AT EL PASO

May 2011

Acknowledgements

I would like to thank Dr. Vinod Kumar, director of Multi-physics Multi-scale Computational Modeling (MU2COM) Laboratory, for giving me the opportunity to perform this research and for the assistance he provided throughout my graduate studies. Dr. Vinod was always available to provide insight and advice for this project. I would also like to thank my other committee member, Dr. Andrzej Pownuk for his assistance during the writing of this thesis.

Part of this research was carried out while I was visiting the National Center of Atmospheric Research (NCAR) in Boulder, CO, U.S.A, as a summer intern. I extend my gratitude to Dr. Ram Nair, scientist at NCAR. Any amount of gratitude expressed to him will remain insufficient. He has been there for me as a good friend who was with me most of the time while I was working on the project. He has taken the effort to understand my problems and support me, and to bring the best in me.

Finally, I would like to thank my family for their support during my graduate studies, who have made my education a high priority from the beginning. Without them, I would not be where I am today.

This thesis was submitted to the supervising committee on May 2011.

Abstract

Atmospheric numerical modeling has been going through drastic changes over the past decade, mainly to utilize the massive computing capability of the petascale systems. This obliges the modelers to develop grid systems and numerical algorithms that facilitate exceptional level of scalability on these systems. The numerical algorithms that can address these challenges should have the local properties such as the high on-processor operation count and minimum parallel communication i.e. high parallel efficiency, it should also satisfy the following properties such as inherent local and global conservation, high-order accuracy, geometric flexibility, non-oscillatory advection, positivity preservation.

In the present work, A Third-order Semi-discrete genuinely multidimensional central scheme for systems of conservation laws and related convection-diffusion equations, is considered to address the challenges mentioned above, this scheme is constructed by Kurganov et al. The construction is based on a multidimensional extension of using more precise information of the local speeds of propagation, and integration over non-uniform control volumes, this scheme is a simple genuinely multidimensional semi-discrete scheme. A two-dimensional piecewise quadratic non-oscillatory reconstruction is employed which ensures the high resolution of the scheme. The scheme is demonstrated for different problems in one-dimension, solid-body rotation and deformational flow tests are considered to test the scheme mentioned above in two-dimensions, some accuracy tests were also performed to test the scheme. The main aim of the project would be to extend the considered scheme to solve compressible Euler equations. Further, to extend the same for Shallow Water model on a cubed sphere.

Table of Contents

List of Tables

List of Figures

Chapter 1: Introduction

In the past few decades, supercomputing in general have evolved enormously. Far from Control Data Corporation's single-operation scalar processors in the 1960s, present day petascale computers that are believed to be capable of performing one quadrillion floating-point operations per second. To utilize the massive computing potential available, atmospheric modelers are obliged to develop grid systems and numerical algorithms that facilitate exceptional level of scalability on these parallel petascale systems. For this reason atmospheric numerical modeling has been going through drastic changes over the past decade [1]. The ideal numerical algorithms that can address these challenges should possess the local properties such as high on-processor operation count and minimum parallel communication i.e. high parallel efficiency, the numerical method should also satisfy the following properties [2] such as:

- Inherent local and global conservation.
- High-order accuracy.
- Geometric flexibility.
- Non-oscillatory advection.
- Positivity preservation.
- Monotonicity.

The discretization schemes for these new generation models are based on finite-volume or spectral-element methods, and using spherical grid system such as the geodesic or cubed-sphere grid that are free from singularities which are prevalent in latitude-longitude type of grid systems at the poles.

A Third-order Semi-discrete genuinely multidimensional central scheme for systems of conservation laws and related convection-diffusion equations, is considered to address the challenges mentioned above, this scheme is constructed by Kurganov et al. [3]. The construction is based on a multidimensional extension of using more precise information of the local speeds of propagation, and integration over non-uniform control volumes.

A two-dimensional piecewise quadratic non-oscillatory reconstruction (see [4]) is employed which ensures the high resolution of the scheme. The scheme considered has the main advantage of the Godunov-type central schemes – simplicity, i.e. it does not employ Riemann solvers [23] and characteristic decomposition; Riemann solvers in general are computationally very expensive. This scheme can be employed as a universal method, which can be easily implemented to a wide variety of problems and can be used as a black-box solver for many multidimensional systems. The scheme is also potential to be computationally efficient and highly scalable to petascale systems, due to the reason that the scheme uses compact stencils to solve the given problem. The scheme is demonstrated for different problems in one-dimension, solid-body rotation and deformational flow tests are considered to test the scheme mentioned above in two-dimensions. The foremost aim of the project would be to extend the considered scheme to solve compressible Euler equations. Further, to extend the same for Shallow Water model on a cubed sphere.

The present material is organized as follows. In chapter 2, we briefly described the background of central schemes and numerical methods considered in atmospheric modeling. In chapter 3, we give an overview of central schemes, Godunov type schemes and the methodology of the scheme (Kurganov et al. [3]) considered for present research work. Results and analysis were mentioned in chapter 4, where we assess the scheme with some standard tests accepted by climate community. In chapter 5, we talk about future work and conclusions. The future work will be accomplished to fulfill the requirements for a doctoral thesis.

Chapter 2: Background

The ensuing material presented in the background has been divided into the following: Firstly a brief introduction and literature review of central schemes is mentioned. Secondly, we talk about numerical methods in atmospheric modeling; here a brief overview of numerical methods considered by modelers in atmospheric modeling is given.

2.1 CENTRAL SCHEMES

Central schemes are used to solve nonlinear convection–diffusion equations, these schemes can be implemented in a straight forward manner as black-box solvers to solve various general conservation laws and related equations governing the spontaneous evolution of large gradient phenomena, therefore the central schemes can be considered as universal finite-difference methods. The central schemes available today are originated from the first-order Lax-Friedrichs scheme, which was developed by Lax [5]. This is a numerical method for the solution of hyperbolic partial differential equations based on finite differences. The method can be described as the forward in time and centered in space (FTCS) scheme. Nessyahu et al. in their work, [6] presented a family of non-oscillatory, second order, central difference approximations to nonlinear systems of hyperbolic conservation laws. These approximations can be viewed as natural extensions of the first-order Lax-Friedrichs (LxF) scheme. This scheme offers high resolution while retaining the simplicity of the Riemann-solver-free approach. Liu et al. developed a third order, non-oscillatory central difference scheme for the approximate solution of non-linear systems of hyperbolic conservation laws [7]. This scheme is the extension of first order Lax-Friedrichs scheme and second order central scheme of Nessayhu and Tadmor (NT).

Kurganov et al., in the their work, [8] introduced a new family of central schemes which admit a particularly simple semi-discrete formulation. The main idea behind the construction is to use more precise information of the local propagation speeds. No characteristic information is required beyond these CFL related speeds. A high-order extension of this scheme, a new third-

order, semi-discrete, central method for approximating solutions to multi-dimensional systems of hyperbolic conservation laws, convection-diffusion equations, and related problems was developed by Kurganov et al. [8]. Kurganov et al. [3] constructed a new third-order semi-discrete genuinely multidimensional central scheme for systems of conservation laws and related convection-diffusion equations. The construction is based on a multidimensional extension of the idea, introduced in [8]. In this scheme more precise information about the local speeds of propagation is used, and integration over non-uniform control volumes, which contain Riemann fans.

2.2 NUMERICAL METHODS IN ATMOSPHERIC MODELING

Over the past two decades Global Spectral Transform methods have dominated in climate simulation [9]. Spherical harmonics spectral methods provide a completely isotropic representation of a scalar function on the sphere with higher accuracy. Global methods based on spherical harmonic basis functions have difficulty exploiting the full potential of current petascale systems, due to the expensive non-local communication operations.

In recent years, researchers have focused on local methods, which adapt favorably for parallel systems [10] [11]. The quest for a positive scheme led to an increase in the popularity of high-order methods, the spectral element (SE) methods that are high-order methods have become more popular during this era [12]. Spectral elements combine the accuracy of conventional spectral methods and the geometric flexibility of finite element methods. The SE method is not inherently conservative [13] because it is not based on conversation laws. For atmospheric applications, the exact conservation of integral invariants such as mass and energy is crucial. It is very crucial to have atmospheric models based on conservative numerical methods; it has been shown that the models that are not based on conservation tend to lose mass over a period of time [14].

Cockburn et al. constructed Discontinuous Galerkin (DG) method, a high-order conservation algorithm for the nonlinear systems of conservation law [15]. Nair et al. developed

a conservative transport scheme on a cubed-sphere using the DG method and extended for the shallow water model [16]. There is a need for a slope limiter in DG method, if the solution contains large discontinuities. There are no known efficient limiters for multidimensional DG methods of polynomial order greater than 4. The capability of the conventional slope limiter to control spurious oscillation diminishes as the order of the polynomial increases [17]. This limits the appliance of high-order DG method in atmospheric modeling.

In atmospheric modeling, finite volume methods are a popular approach, these methods that ensure conservation in atmospheric models. It treats the equations in flux form with control volumes, obtaining conservation through careful discretization of the control volume fluxes. Wang and Liu [18] [19] developed a conservative high-order spectral finite volume (SFV) method for the solution of two-dimensional systems of conservation laws. SFV method is based on classical finite volume scheme and applied to each cell appearing in a spectral element, with the reconstruction based on a high-order method. It is easy to incorporate traditional multidimensional limiters in a finite volume approach. Choi et al. [20] developed a SFV method for the numerical solution of the shallow water equations. A flux-corrected transport (FCT) scheme is incorporated to enforce monotonicity near strong discontinuities or under-resolved gradients. Vani et al. [21], in their work developed a SFV scheme for transport equation. SFV scheme employs rectangular elements with high-order nodal discretization based on Gauss–Lobatto–Legendre points [22]. A third-order explicit strong stability preserving time integration scheme was used.

Chapter 3: Overview of the Central Schemes and Methodology

3.1 INTRODUCTION

Kurganov et al. constructed a third-order semi-discrete genuinely multidimensional central scheme for systems of conservation laws and related convection-diffusion equations [3]. We consider this scheme to apply it in atmospheric modeling; in the present work presented here we test the considered scheme using some standard tests accepted by climate community. The construction is based on a multidimensional extension of the idea, introduced in [8]. This scheme is a simple genuinely multidimensional semi-discrete scheme, Two-dimensional piecewise quadratic non-oscillatory reconstruction ensures the high resolution of this scheme. The advantages of this scheme include the simplicity, the main advantage of Godunov type central schemes. It does not contain Reimann solvers [23], which are computationally very expensive, and also does not have characteristic decomposition.

The material in this chapter is divided into the following: we describe the Godunov type central schemes and later we elucidate the methodology of the scheme considered (Kurganov et al. [3]). Brief description about the limiter and time integration method employed in the present work is also mentioned in this chapter.

3.2 GODUNOV TYPE SCHEMES

Godunov's scheme is a conservative numerical scheme, developed by S. K. Godunov [23], for solving partial differential equations. These schemes are projection-evolution methods, the conservative variables are considered as piecewise constant over the grid cells at every time step and the time evolution is determined by the exact solution of the Riemann problem at the inter-cell boundaries [25]. There are three consecutive stages at every time step:

1. Reconstruction: Piecewise constant data (the cell-averages) is computed at the previous time step from which a piecewise polynomial interpolant is reconstructed.

2. Evolution: The reconstructed interpolant is evolved in time according to considered conservation laws.
3. Projection: The solution is then projected onto a space of piecewise constants.

Depending on the final step (projection) these schemes are classified into two types:

1. Upwind: Characteristic decomposition and Riemann solver are involved. E.g. Monotone Upstream-centered Schemes for Conservation Laws (MUSCL), Piecewise parabolic Method (PPM), weighted essentially non-oscillatory (WENO)
2. Central: Exact evolution and averaging over Riemann fans, characteristic decomposition and Riemann solver are not involved, this type requires a staggered grid system. E.g. Lax-Friedrichs scheme [5, 25], NT [6], higher order generalizations of NT [4, 26, 27], 2-order multidimensional central schemes [28, 29], the higher order extensions of these are given in [30, 31]

Therefore this makes the Godunov type central schemes simple and universal methods, and can also be used as black-box solvers for many multidimensional systems. The advantage of the higher-order schemes is that they reduce the excessive numerical viscosity, typical for the Lax-Friedrichs scheme, and give much sharper resolution of the shocks and rarefactions.

The examples given for central schemes do not provide good resolution when small steps are enforced, and they do not admit semi-discrete form. These difficulties are resolved in the scheme constructed in KT [8], In the new construction of this scheme, the evolution step is executed by integrating over non-equal control volumes, here the sizes are proportional to the local speeds of propagation. The evolved solution is then projected back onto the original grid, which requires an additional piecewise polynomial reconstruction. This ensures, a non-staggered fully-discrete central scheme. This is therefore reduced to a semi-discrete scheme. The multi-dimensional semi-discrete scheme in KT [8] was obtained by so called dimension-by-dimension approach. Kurganov et al. [3] developed a high order genuinely multidimensional semi-discrete central scheme based on multidimensional generalization of the one-dimensional construction

from KT [8]. In general semi-discrete schemes consist of three steps: firstly piecewise polynomial reconstruction, and then flux discretization spatially and finally an Ordinary Differential Equation (ODE) solver. The scheme constructed by Kurganov et al. [3] provides the fluxes. For reconstruction purpose we can choose any from the available non-oscillatory reconstruction schemes such as [32, 33, 34, 35, 6, 36], to build a third-order accurate scheme, one can use essentially non-oscillatory (ENO) or weighted essentially non-oscillatory (WENO) reconstruction [33, 37, 38, 39, 27]. Kurganov et al. [3] in their scheme used a less dissipative one-dimensional modification of the reconstruction of [4]. The two-dimensional numerical fluxes are obtained from the generalization of one-dimensional reconstruction.

3.3 GOVERNING EQUATIONS

In this project we are interested in solving the multidimensional system of conservation laws, the equations that are considered are as follows:

One-dimension scalar conservation law:

$$u_t + \nabla_{\mathrm{x}} \cdot f(u) = 0 \qquad (1)$$

here

$$\mathrm{x} \in \mathbb{R}^d$$

Convection-diffusion equation is given by:

$$u_t + \nabla_{\mathrm{x}} \cdot f(u) = \nabla_{\mathrm{x}} Q(u, \nabla_{\mathrm{x}} u) \qquad (2)$$

where Q satisfies the condition

$$\nabla_{\mathrm{x}} Q(u, s) \geq 0 \qquad \forall (u, s)$$

The initial data is considered as:

$$u(\mathrm{x}, 0) = u_0(\mathrm{x}) \qquad (3)$$

we considered linear advection for simplicity, and is given by:

$$f(u) = cu$$

3.3.1 Third-Order Semi-Discrete Non-Oscillatory Scheme for conservation laws

The sliding average is defined by the following expression:

$$\bar{u}(x,t) := \frac{1}{\Delta x}\int_{I(x)} u(\xi,t)d\xi \qquad (4)$$

where:

$$I(x) = \{\xi : |\xi - x| < \frac{\Delta x}{2}\} \qquad (5)$$

Equation (1) is integrated over (5) X [t, t+Δt], and the resultant equation, which is equivalent to (1), we arrive at the starting point for the construction of Godunov type schemes, the resulting equation is as follows:

$$\bar{u}(x,t+\Delta t) = \bar{u}(x,t) - \frac{1}{\Delta x} \times \left[\int_{\tau=t}^{t+\Delta t} f(u(x+\frac{\Delta x}{2},\tau))d\tau - \int_{\tau=t}^{t+\Delta t} f(u(x-\frac{\Delta x}{2},\tau))d\tau\right] \qquad (6)$$

Reconstruction:

First step is the reconstruction, in this step a piecewise polynomial function is reconstructed from the data which is computed at the previous time step, at time level $t = t^n$.

Piecewise polynomial function is given by the following equation:

$$\tilde{u}(x,t^n) = p_j^n(x)$$

where the algebraic polynomials are defined by: p_j^n

The illustration of piecewise linear construction can be seen in figure 2.1

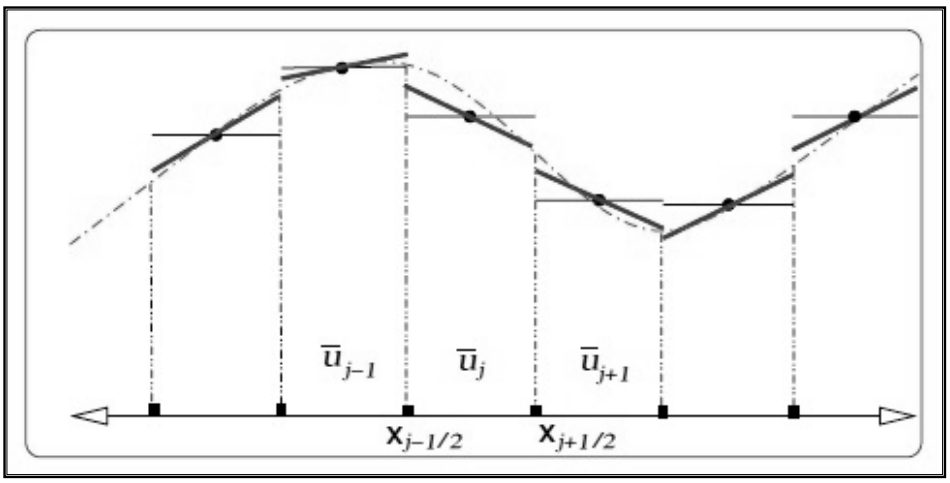

Figure 3.1: Schematic illustration of piecewise linear construction

In figure 2.1 (© R. Nair) the cell averages u, are shown as horizontal lines and the cell boundaries are labeled by $x_{j\pm\frac{1}{2}}$. The smooth dashed line indicates the actual solution $u(x)$ which is approximated by piecewise linear distributions on each cell.

The cell width is given by the following expression:

$$\Delta x_j = x_{j+\frac{1}{2}} - x_{j-\frac{1}{2}}$$

The reconstruction procedure should satisfy the following properties:

1. Conservation of the considered cell averages

$$\int_{x_{j-\frac{1}{2}}}^{x_{j+\frac{1}{2}}} (\zeta, t^n) d\zeta = \bar{u}_j^n, \qquad \forall j$$

2. For smooth $u(x,t)$, the accuracy

$$\tilde{u}(x, t^n) = u(x, t^n) + O((\Delta x)^r)$$

where r is the order of the scheme.

The second step in the procedure is the Evolution step, in this step the piecewise polynomial $u\tilde{}(\bullet,t)$ is evolved exactly according to the equation (6) and the solution is obtained at time $t = t^{n+1}$, the solution thus obtained is in terms of sliding averages.

The final step is the projection, this is done by the evaluation of the sliding averages (obtained in evolution step) at the particular grid points, this gives us the approximate cell averages of the solution at the next time step.

The equation (6) therefore leads to so called Godunov type central scheme and is given by:

$$\bar{u}_{n-1}^{n+1} = \frac{1}{\Delta x}\left[\int_{x_j}^{x_{j+1/2}} p_j^n(x)dx + \int_{x_{j+1/2}}^{x_{j+1}} p_{j+1}^n(x)dx\right] - \frac{\lambda}{\Delta t}\left[\int_{t^n}^{t^{n+1}} f\left(u(x_{j+1},t)\right)dt - \int_{t^n}^{t^{n+1}} f\left(u(x_j,t)\right)dt\right]$$

Here $\lambda = \Delta t/\Delta x$.

The RHS of the equation mentioned above can be evaluated easily compared to the upwind schemes, which saves a lot of computation time. Using a quadrature formula, whose order should be greater than the order of the scheme constructed, can approximate the flux integrals in the above equation. The function values, which are needed in the quadrature can be computed using Runge-Kutta method [40].

Time Integration

There are many known time integrators available that one can use to solve the differential equation in above expression. In this work we use a strong stability preserving third order Runge-Kutta (SSP-RK) time integration [40]. SSP time integration schemes are widely used in DG literature [15], these schemes do not generate new local maxima or minima due to time discretization. For this very reason we consider SSP third-order Runge–Kutta time integration scheme for the method considered. For a given ordinary differential equation,

$$\frac{d}{dt}U = L(U) \quad in(0,T)$$

the third order SSP-RK scheme is given by the following set of equation:

$$\overline{U}^{(1)} = [\overline{U}^n + \Delta t L(\overline{U}^n],$$
$$\overline{U}^{(2)} = \frac{3}{4}\overline{U}^n + \frac{1}{4}\left[\overline{U}^{(1)} + \Delta t L(\overline{U}^{(1)}\right],$$

$$\overline{U}^{(n+1)} = \frac{1}{4}\overline{U}^{n} + \frac{2}{3}\left[\overline{U}^{(2)} + \Delta t L(\overline{U}^{(2)}\right]$$

Here the superscripts n denotes the time level t and $n+1$ denotes the time level $t + \Delta t$.

Minmod Limiter:

The above-mentioned SSP-RK scheme is suitable when the solution is smooth, but if the solution contains strong shocks or discontinuities, oscillations that lead to non-linear instabilities will appear. A SSP-RK scheme cannot alone control such undesirable effects; therefore a slope limiter is required after each step of SSP-RK time integration. Minmod limiter [41] is used in our work to control these spurious oscillations. The slopes are given by:

$$s_j^n = \text{minmod}\left(\frac{\bar{u}_j^n - \bar{u}_{j-1}^n}{\Delta x}, \frac{\bar{u}_{j+1}^n - \bar{u}_j^n}{\Delta x}\right)$$

$s^n{}_j$ are the slopes and

$$\text{minmod}(a,b) := \frac{sgn(a) + sgn(b)}{2}\min\left(|a|, |b|\right)$$

Semi-Discrete Central Scheme in One-Dimension:

The first step in the process is piecewise polynomial reconstruction $p^n{}_j$, there may be some discontinuities at the interface points $x_{j+1/2}$, these discontinuities (shown in Figure 3.3) may propagate at different speeds, these speeds for genuinely nonlinear or non-linear degenerate case may be:

$$a_{j+\frac{1}{2}}^n := max\left\{\rho\left(\frac{\partial f}{\partial u}\left(u_{j+\frac{1}{2}}^{n-}\right)\right), \rho\left(\frac{\partial f}{\partial u}\left(u_{j+\frac{1}{2}}^{n+}\right)\right)\right\}$$

The Domain Ω (Periodic) is partitioned into Nx Non-Overlapping cells. We can see the partitioning in the Figure 3.2:

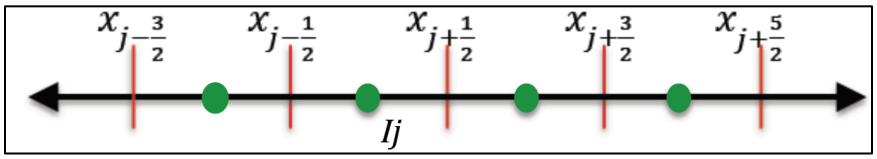

Figure 3.2: Schematic illustration of domain decomposition.

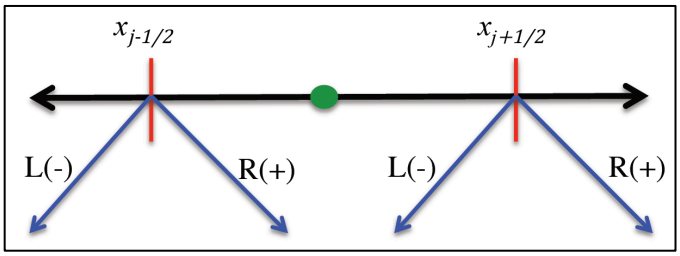

Figure 3.3: Illustration of possible discontinuities at the interfaces.

where:

$$I_j = \left[x_{j-\frac{1}{2}}, x_{j+\frac{1}{2}}\right] \qquad j = 1, \ldots, N_x \qquad \Delta x_j = \left(x_{j+\frac{1}{2}} - x_{j-\frac{1}{2}}\right)$$

The semi discrete formulation can be achieved in the following way, substitute $\boldsymbol{u}^{n+1}{}_j$ (from fully discrete scheme) in the following expression:

$$\frac{d}{dt}\bar{u}_j(t) = \lim_{\Delta t \to 0}\left(\frac{\bar{u}_j^{n+1} - \bar{u}_j^n}{\Delta t}\right)$$

here Δx is fixed, the r^{th} order semi discrete scheme is derived and can be represented as:

$$\frac{d}{dt}\bar{u}_j(t) = \frac{H_{j+\frac{1}{2}}(t) - H_{j-\frac{1}{2}}(t)}{\Delta x}$$

Here H is numerical flux and is given by:

$$H_{j+\frac{1}{2}}(t) := \frac{f\left(u^+_{j+\frac{1}{2}}(t)\right) + f\left(u^-_{j+\frac{1}{2}}(t)\right)}{2} - \frac{a_{j+\frac{1}{2}}(t)}{2}\left[u^+_{j+\frac{1}{2}}(t) - u^-_{j+\frac{1}{2}}(t)\right]$$

where $u^{+-}{}_{j+1/2}$, are the cell intermediate values and can be defined in the following way:

$$u^+_{j+\frac{1}{2}} := p_{j+1}\left(x_{j+\frac{1}{2}}\right), \qquad u^-_{j+\frac{1}{2}} := p_j\left(x_{j+\frac{1}{2}}\right)$$

Here p_j is the r^{th} order piecewise polynomial reconstruction at time t. We refer the reader to see Kurganov et al. [3] for all the details and derivations. The reconstruction pnj can be calculated from:

$$p_j^n(x) = (1-\theta_j^n)L_j^n(x) + \theta_j^n q_j^n(x)$$

Here $L^n{}_j$ is the linear interpolant, $q^n{}_j$ is basic piecewise quadratic function, and are given by:

$$L_j^n(x) = \bar{u}_j^n + s_j^x(x - x_j)$$

$$q_j^n(x) = \left(\bar{u}_j^n - \frac{(\Delta x)^2}{24} D_+ D_- \bar{u}_j^n\right) + D_0 \bar{u}_j^n (x - x_j) + \frac{1}{2} D_+ D_- \bar{u}_j^n (x - x_j)^2$$

The non-oscillatory property of the piecewise quadratic reconstruction is ensured by $\theta^n{}_j$ and is given by:

$$\theta := \begin{cases} min\left\{\dfrac{M_{j+\frac{1}{2}}^n - L_j^n\left(x_{j+\frac{1}{2}}\right)}{M_j^n - L_j^n\left(x_{j+\frac{1}{2}}\right)}, \dfrac{m_{j-\frac{1}{2}}^n - L_j^n\left(x_{j-\frac{1}{2}}\right)}{m_j^n - L_j^n\left(x_{j-\frac{1}{2}}\right)}, 1\right\} & if\ \bar{u}_{j-1}^n < \bar{u}_j^n < \bar{u}_{j+1}^n, \\ min\left\{\dfrac{M_{j-\frac{1}{2}}^n - L_j^n\left(x_{j-\frac{1}{2}}\right)}{M_j^n - L_j^n\left(x_{j-\frac{1}{2}}\right)}, \dfrac{m_{j+\frac{1}{2}}^n - L_j^n\left(x_{j+\frac{1}{2}}\right)}{m_j^n - L_j^n\left(x_{j+\frac{1}{2}}\right)}, 1\right\} & if\ \bar{u}_{j-1}^n > \bar{u}_j^n > \bar{u}_{j+1}^n, \\ 1. & else \end{cases}$$

where

$$M_j^n = max\left\{q_j^n\left(x_{j+\frac{1}{2}}\right) - q_j^n\left(x_{j-\frac{1}{2}}\right)\right\}$$

$$m_j^n = min\left\{q_j^n\left(x_{j+\frac{1}{2}}\right) - q_j^n\left(x_{j-\frac{1}{2}}\right)\right\}$$

$$M_{j\pm\frac{1}{2}}^n = max\left\{\frac{1}{2}\left(L_j^n\left(x_{j\pm\frac{1}{2}}\right) + L_{j\pm1}^n\left(x_{j\pm\frac{1}{2}}\right)\right), q_{j\pm1}^n\left(x_{j\pm\frac{1}{2}}\right)\right\}$$

$$m_{j\pm\frac{1}{2}}^n = min\left\{\frac{1}{2}\left(L_j^n\left(x_{j\pm\frac{1}{2}}\right) + L_{j\pm1}^n\left(x_{j\pm\frac{1}{2}}\right)\right), q_{j\pm1}^n\left(x_{j\pm\frac{1}{2}}\right)\right\}$$

This new reconstruction is less dissipative and allows has to have better resolution.

A Genuinely Multi-Dimensional Third-Order Semi-Discrete Scheme:

The one-dimesional case mentioned above is generalized for multi-dimensional case. The two-dimensional case for system of hyperbolic conservation laws is given.

$$u_t + f(u)_x + g(u)_y = 0$$

The cell averages is defined by the following equation:

$$\bar{u}_{j,k} := \frac{1}{\Delta x \Delta y} \int_{x_{j-\frac{1}{2}}}^{x_{j+\frac{1}{2}}} \int_{y_{k-\frac{1}{2}}}^{y_{k+\frac{1}{2}}} p_{j,k}^{n}(x,y)dxdy$$

The corresponding point values are determined as:

$u_{j,k} := p_{j,k}^{n}(x_j, y_k)$, $\quad u_{j,k}^{N} := p_{j,k}^{n}\left(x_j, y_{k+\frac{1}{2}}\right)$,

$u_{j,k}^{S} := p_{j,k}^{n}\left(x_j, y_{k-\frac{1}{2}}\right)$, $\quad u_{j,k}^{E} := p_{j,k}^{n}\left(x_{j+\frac{1}{2}}, y_k\right)$,

$u_{j,k}^{W} := p_{j,k}^{n}\left(x_{j-\frac{1}{2}}, y_k\right)$, $\quad u_{j,k}^{NE} := p_{j,k}^{n}\left(x_{j+\frac{1}{2}}, y_{k+\frac{1}{2}}\right)$,

$u_{j,k}^{NW} := p_{j,k}^{n}\left(x_{j-\frac{1}{2}}, y_{k+\frac{1}{2}}\right)$, $\quad u_{j,k}^{SE} := p_{j,k}^{n}\left(x_{j+\frac{1}{2}}, y_{k-\frac{1}{2}}\right)$,

$u_{j,k}^{SW} := p_{j,k}^{n}\left(x_{j-\frac{1}{2}}, y_{k-\frac{1}{2}}\right)$.

The local speeds of propagation are given by:

$$a_{j+\frac{1}{2},k}^{x} := max\left\{\rho\left(\frac{\partial f}{\partial u}\left(x_{j+1,k}^{W}\right)\right), \rho\left(\frac{\partial f}{\partial u}\left(x_{j,k}^{E}\right)\right)\right\}$$

$$a_{j,k+\frac{1}{2}}^{y} := max\left\{\rho\left(\frac{\partial g}{\partial u}\left(x_{j,k+1}^{S}\right)\right), \rho\left(\frac{\partial g}{\partial u}\left(x_{j,k}^{N}\right)\right)\right\}$$

In the process of deriving the new genuinely multidimensional semi-discrete scheme, the first step is:

$$\frac{d}{dt}\bar{u}_{j,k}(t) = \lim_{\Delta t \to 0}\left(\frac{\bar{u}_{j,k}^{n+1} - \bar{u}_{j,k}^{n}}{\Delta t}\right)$$

We recommend for the reader to refer to Kurganov et al. [3], for the description and derivation of the scheme. The new semi discrete scheme is represented by:

$$\frac{d}{dt}\bar{u}_{j,k}(t) = \frac{H_{j+\frac{1}{2},k}^{x}(t) - H_{j-\frac{1}{2},k}^{x}(t)}{\Delta x} - \frac{H_{j,k+\frac{1}{2}}^{y}(t) - H_{j,k-\frac{1}{2}}^{y}(t)}{\Delta y}$$

wher the numerical fluxes are given by:

$$H_{j+\frac{1}{2},k}^{x}(t):$$

$$= \frac{\left\{f\left(u_{j+1,k}^{NW}(t)\right) + f\left(u_{j,k}^{NE}(t)\right) + 4\left(f\left(u_{j+1,k}^{W}(t)\right) + f\left(u_{j,k}^{E}(t)\right)\right) + f\left(u_{j+1,k}^{SW}(t)\right) + f\left(u_{j,k}^{SE}(t)\right)\right\}}{\{12\}}$$

$$- \frac{a_{j+\frac{1}{2},k}^{x}(t)}{12} \times \left[u_{j+1,k}^{NW}(t) - u_{j,k}^{NE}(t) + 4\left(u_{j,k+1}^{W}(t) - u_{j,k}^{E}(t)\right) + u_{j+1,k}^{SW}(t) - u_{j,k}^{SE}(t)\right]$$

$$H^{y}_{j,k+\frac{1}{2}}(t):$$

$$= \frac{\left\{g\left(u^{SW}_{j,k+1}(t)\right) + g\left(u^{NW}_{j,k}(t)\right) + 4\left(g\left(u^{S}_{j,k+1}(t)\right) + g\left(u^{N}_{j,k}(t)\right)\right) + g\left(u^{SE}_{j,k+1}(t)\right) + g\left(u^{NE}_{j,k}(t)\right)\right\}}{\{12\}}$$

$$- \frac{a^{y}_{j,k+\frac{1}{2}}(t)}{12} \times \left[u^{SW}_{j,k+1}(t) - u^{NW}_{j,k}(t) + 4\left(u^{S}_{j,k+1}(t) - u^{N}_{j,k}(t)\right) + u^{SE}_{j,k+1}(t) - u^{NE}_{j,k}(t)\right]$$

The eight point values $u^{N}_{j,k}$, $u^{E}_{j,k}$, $u^{S}_{j,k}$, $u^{W}_{j,k}$, $u^{NE}_{j,k}$, $u^{NW}_{j,k}$, $u^{SE}_{j,k}$, $u^{SW}_{j,k}$, are required to compute the numerical fluxes determined above, this is done in two individual steps first the values in coordinate direction and the secondly the values in diagonal direction are computed. These values are defined by using 'dimension-by-dimension' approach.

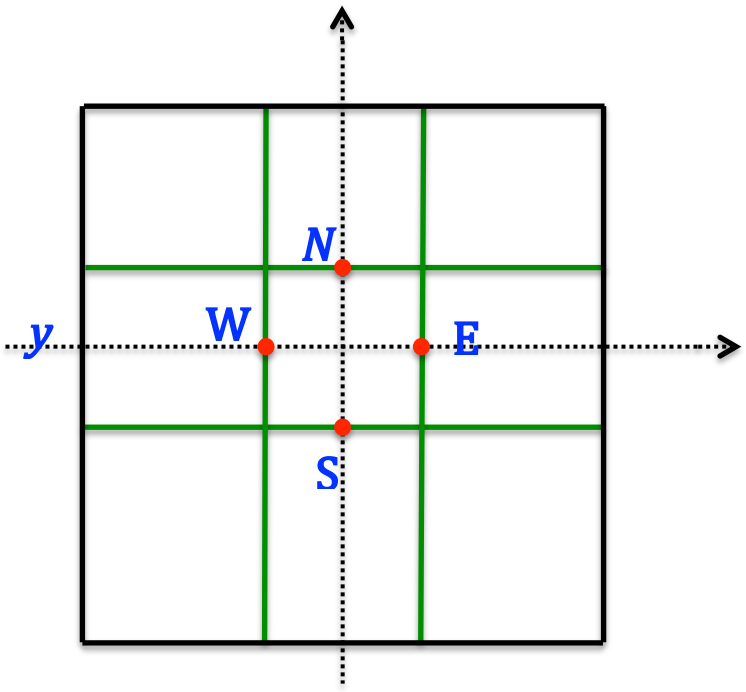

Figure 3.4: Reconstruction in *x* and *y* directions.

The point values ($u^{N}_{j,k}$, $u^{E}_{j,k}$, $u^{S}_{j,k}$, $u^{W}_{j,k}$) in the coordinate directions (above figure) are computed using the following equations:

$$p^{n}_{j,k}(x,y) = (1-\theta^{n}_{j,k})L^{n}_{j,k}(x,y) + \theta^{n}_{j,k}q^{n}_{j,k}(x,y)$$
$$0 < \theta^{n}_{j,k} < 1$$

Here

$$\theta_{j,k}^{n} = \min\{\theta_{j,k}^{x}, \theta_{j,k}^{y}\}$$

and the values of $\theta^{x}_{j,k}$, $\theta^{y}_{j,k}$ are given by values defined in one-dimensional case above.

The basic parabolas are given by:

$$q_{j,k}^{n}(x,y) = \left(\bar{u}_{j,k}^{n} - \frac{(\Delta x)^2}{24} D_{+}^{x} D_{-}^{x} \bar{u}_{j,k}^{n} - \frac{(\Delta y)^2}{24} D_{+}^{y} D_{-}^{y} \bar{u}_{j,k}^{n}\right) + D_{0}^{x} \bar{u}_{j,k}^{n}(x - x_j) + D_{0}^{y} \bar{u}_{j,k}^{n}(y - y_k)$$
$$+ \frac{1}{2} D_{+}^{x} D_{-}^{x} \bar{u}_{j,k}^{n}(x - x_j)^2 + \frac{1}{2} D_{+}^{y} D_{-}^{y} \bar{u}_{j,k}^{n}(y - y_k)^2 + D_{0}^{x} D_{0}^{y} \bar{u}_{j,k}^{n}(x - x_j)(y - y_k)$$

where:

$$D_{\pm}^{x} v(x,y) \coloneqq \pm \frac{v(x \pm \Delta x, y) - v(x,y)}{\Delta x}$$
$$D_{\pm}^{y} v(x,y) \coloneqq \pm \frac{v(x, y \pm \Delta y) - v(x,y)}{\Delta y}$$
$$D_{0}^{x} v(x,y) \coloneqq \frac{v(x + \Delta x, y) - v(x - \Delta x, y)}{2\Delta x}$$
$$D_{0}^{y} v(x,y) \coloneqq \frac{v(x, y + \Delta y) - v(x, y - \Delta y)}{2\Delta y}$$

The piecewise linear functions are:

$$L_{j,k}^{n}(x,y) = \bar{u}_{j,k}^{n} + s_{j,k}^{x}(x - x_j) + s_{j,k}^{y}(y - y_k)$$

The slopes are given by:

$$s_{j,k}^{x} = minmod\left(\frac{\bar{u}_{j,k}^{n} - \bar{u}_{j-1,k}^{n}}{\Delta x}, \frac{\bar{u}_{j+1,k}^{n} - \bar{u}_{j,k}^{n}}{\Delta x}\right)$$
$$s_{j,k}^{y} = minmod\left(\frac{\bar{u}_{j,k}^{n} - \bar{u}_{j,k-1}^{n}}{\Delta y}, \frac{\bar{u}_{j,k+1}^{n} - \bar{u}_{j,k}^{n}}{\Delta y}\right)$$

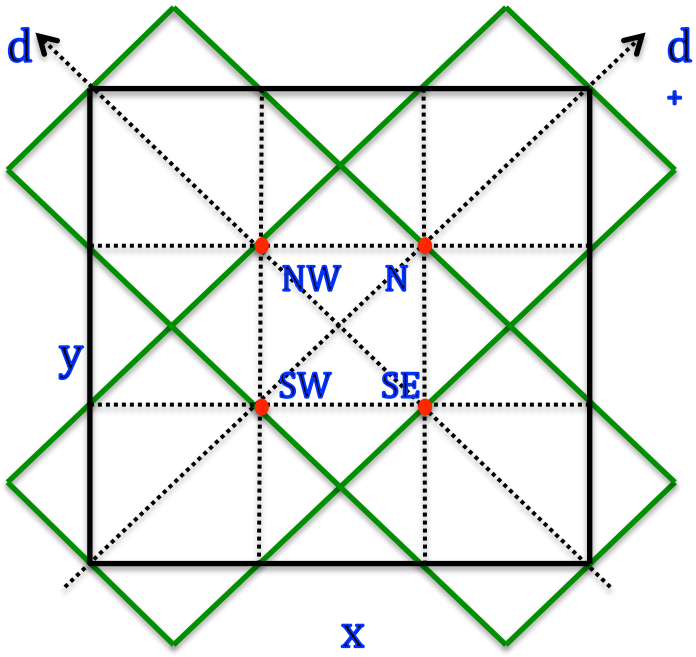

Figure 3.5: Reconstruction in diagonal directions.

The computation of diagonal point values ensures there are no oscillations in the diagonal direction, and also ensures there is no loss of dissipation in the diagonal direction unlike the conventional FV methods.

The reconstruction is given by the piecewise polynomial function in the following expression:

$$\hat{p}_{j,k}^{n}(x,y) = (1-\hat{q}_{j,k}^{n})\hat{L}_{j,k}^{n}(x,y) + \hat{\theta}_{j,k}^{n}\hat{q}_{j,k}^{n}(x,y)$$
$$0 < \hat{\theta}_{j,k}^{n} < 1$$

The basic parabolas for the diagonal directions are given by:

$$\hat{q}_{j,k}^{n}(x,y) = \left(\bar{u}_{j,k}^{n} - \frac{(\Delta)^2}{48} D_{+}^{d+} D_{-}^{d+} \bar{u}_{j,k}^{n} - \frac{(\Delta)^2}{48} D_{+}^{d-} D_{-}^{d-} \bar{u}_{j,k}^{n}\right)$$
$$+ D_{0}^{d+} \bar{u}_{j,k}^{n} \left(\frac{\Delta}{2\Delta \mathrm{y}} (y - y_k) + \frac{\Delta}{2\Delta \mathrm{x}} (x - x_j)\right)$$
$$+ D_{0}^{d-} \bar{u}_{j,k}^{n} \left(\frac{\Delta}{2\Delta \mathrm{y}} (y - y_k) - \frac{\Delta}{2\Delta \mathrm{x}} (x - x_j)\right)$$
$$+ D_{0}^{d+} D_{0}^{d-} \bar{u}_{j,k}^{n} \left(\frac{\Delta^2}{4(\Delta \mathrm{y})^2} (y - y_k)^2 - \frac{\Delta^2}{4(\Delta \mathrm{x})^2} (x - x_j)^2\right)$$
$$+ \frac{1}{2} D_{+}^{d+} D_{-}^{d+} \bar{u}_{j,k}^{n} \left(\frac{\Delta}{2\Delta \mathrm{y}} (y - y_k) + \frac{\Delta}{2\Delta \mathrm{x}} (x - x_j)\right)^2$$
$$+ \frac{1}{2} D_{+}^{d-} D_{-}^{d-} \bar{u}_{j,k}^{n} \left(\frac{\Delta}{2\Delta \mathrm{y}} (y - y_k) - \frac{\Delta}{2\Delta \mathrm{x}} (x - x_j)\right)^2$$

where

$\Delta \coloneqq \sqrt{(\Delta \mathrm{x})^2 + (\Delta \mathrm{y})^2}$

and the divided differences for the diagonal directions are given by:

$$D_{\pm}^{d+} v(x,y) \coloneqq \pm \frac{v(x \pm \Delta x, y \pm \Delta y) - v(x,y)}{\Delta}$$
$$D_{\pm}^{d-} v(x,y) \coloneqq \pm \frac{v(x \mp \Delta x, y \pm \Delta y) - v(x,y)}{\Delta}$$
$$D_{0}^{d+} v(x,y) \coloneqq \frac{v(x + \Delta x, y + \Delta y) - v(x - \Delta x, y - \Delta y)}{2\Delta}$$
$$D_{0}^{y} v(x,y) \coloneqq \frac{v(x - \Delta x, y + \Delta y) - v(x + \Delta x, y - \Delta y)}{2\Delta}$$

The linear functions for the diagonal directions are given by:

$$\hat{L}_{j,k}^{n}(x,y) = \hat{u}_{j,k}^{n} + \hat{s}_{j,k}^{+} \left[\frac{\Delta}{2\Delta \mathrm{y}} (y - y_k) + \frac{\Delta}{2\Delta \mathrm{x}} (x - x_j)\right]$$
$$+ \hat{s}_{j,k}^{-} \left[\frac{\Delta}{2\Delta \mathrm{y}} (y - y_k) - \frac{\Delta}{2\Delta \mathrm{x}} (x - x_j)\right]$$

The slopes in the diagonal direction are given by:

$$\hat{s}_{j,k}^{+} = minmod\left(\frac{\bar{u}_{j,k}^{n} - \bar{u}_{j-1,k-1}^{n}}{\Delta}, \frac{\bar{u}_{j+1,k+1}^{n} - \bar{u}_{j,k}^{n}}{\Delta}\right)$$
$$\hat{s}_{j,k}^{-} = minmod\left(\frac{\bar{u}_{j,k}^{n} - \bar{u}_{j+1,k+1}^{n}}{\Delta}, \frac{\bar{u}_{j-1,k+1}^{n} - \bar{u}_{j,k}^{n}}{\Delta}\right)$$

where

$\hat{\theta}_{j,k}^{n} = \min\{\hat{\theta}_{j,k}^{+}, \hat{\theta}_{j,k}^{-}\}$

$$\theta_{j,k}^{\pm} := \begin{cases} min\left\{\dfrac{M_{j\pm\frac{1}{2},k+\frac{1}{2}}^{\pm} - \hat{L}_{j,k}^{n}\left(x_{j\pm\frac{1}{2}}, y_{k+\frac{1}{2}}\right)}{M_{j,k}^{\pm} - \hat{L}_{j}^{n}\left(x_{j\pm\frac{1}{2}}, y_{k+\frac{1}{2}}\right)}, \dfrac{m_{j\mp\frac{1}{2},k-\frac{1}{2}}^{\pm} - \hat{L}_{j,k}^{n}\left(x_{j\mp\frac{1}{2}}, y_{k-\frac{1}{2}}\right)}{m_{j,k}^{\pm} - \hat{L}_{j,k}^{n}\left(x_{j\mp\frac{1}{2}}, y_{k-\frac{1}{2}}\right)}, 1\right\} \\ if\ \bar{u}_{j\mp1,k-1}^{n} < \bar{u}_{j,k}^{n} < \bar{u}_{j\pm1,k+1}^{n}, \\ min\left\{\dfrac{M_{j\mp\frac{1}{2},k-\frac{1}{2}}^{\pm} - \hat{L}_{j,k}^{n}\left(x_{j\mp\frac{1}{2}}, y_{k-\frac{1}{2}}\right)}{M_{j,k}^{\pm} - \hat{L}_{j}^{n}\left(x_{j\mp\frac{1}{2}}, y_{k-\frac{1}{2}}\right)}, \dfrac{m_{j\pm\frac{1}{2},k+\frac{1}{2}}^{\pm} - \hat{L}_{j,k}^{n}\left(x_{j\pm\frac{1}{2}}, y_{k+\frac{1}{2}}\right)}{m_{j,k}^{\pm} - \hat{L}_{j,k}^{n}\left(x_{j\pm\frac{1}{2}}, y_{k+\frac{1}{2}}\right)}, 1\right\} \\ if\ \bar{u}_{j\mp1,k-1}^{n} > \bar{u}_{j,k}^{n} > \bar{u}_{j\pm1,k+1}^{n}, \\ 1. \qquad else \end{cases}$$

where

$$M_{j,k}^{\pm} = \max\left\{\hat{q}_{j,k}^{n}\left(x_{j\pm\frac{1}{2}}, y_{k+\frac{1}{2}}\right), \hat{q}_{j,k}^{n}\left(x_{j\mp\frac{1}{2}}, y_{k-\frac{1}{2}}\right)\right\}$$

$$m_{j,k}^{\pm} = \min\left\{\hat{q}_{j,k}^{n}\left(x_{j\pm\frac{1}{2}}, y_{k+\frac{1}{2}}\right), \hat{q}_{j,k}^{n}\left(x_{j\mp\frac{1}{2}}, y_{k-\frac{1}{2}}\right)\right\}$$

$$M_{j\pm\frac{1}{2},k\pm\frac{1}{2}}^{+} = \max\left\{\frac{1}{2}\left(\hat{L}_{j,k}^{n}\left(x_{j\pm\frac{1}{2}}, y_{k\pm\frac{1}{2}}\right) + \hat{L}_{j\pm1,k\pm1}^{n}\left(x_{j\pm\frac{1}{2}}, y_{k\pm\frac{1}{2}}\right)\right), \hat{q}_{j\pm1,k\pm1}^{n}\left(x_{j\pm\frac{1}{2}}, y_{k\pm\frac{1}{2}}\right)\right\}$$

$$M_{j\mp\frac{1}{2},k\pm\frac{1}{2}}^{-} = \max\left\{\frac{1}{2}\left(\hat{L}_{j,k}^{n}\left(x_{j\mp\frac{1}{2}}, y_{k\pm\frac{1}{2}}\right) + \hat{L}_{j\mp1,k\pm1}^{n}\left(x_{j\mp\frac{1}{2}}, y_{k\pm\frac{1}{2}}\right)\right), \hat{q}_{j\mp1,k\pm1}^{n}\left(x_{j\mp\frac{1}{2}}, y_{k\pm\frac{1}{2}}\right)\right\}$$

$$m_{j\pm\frac{1}{2},k\pm\frac{1}{2}}^{+} = \min\left\{\frac{1}{2}\left(\hat{L}_{j,k}^{n}\left(x_{j\pm\frac{1}{2}}, y_{k\pm\frac{1}{2}}\right) + \hat{L}_{j\pm1,k\pm1}^{n}\left(x_{j\pm\frac{1}{2}}, y_{k\pm\frac{1}{2}}\right)\right), \hat{q}_{j\pm1,k\pm1}^{n}\left(x_{j\pm\frac{1}{2}}, y_{k\pm\frac{1}{2}}\right)\right\}$$

$$m_{j\mp\frac{1}{2},k\pm\frac{1}{2}}^{-} = \min\left\{\frac{1}{2}\left(\hat{L}_{j,k}^{n}\left(x_{j\mp\frac{1}{2}}, y_{k\pm\frac{1}{2}}\right) + \hat{L}_{j\mp1,k\pm1}^{n}\left(x_{j\mp\frac{1}{2}}, y_{k\pm\frac{1}{2}}\right)\right), \hat{q}_{j\mp1,k\pm1}^{n}\left(x_{j\mp\frac{1}{2}}, y_{k\pm\frac{1}{2}}\right)\right\}$$

Chapter 4: Results and Analysis

4.1 NUMERICAL TESTS ONE-DIMENSION CASE

In this section we illustrate the scheme considered [3] by solving two examples of the one-dimensional conservation law. The first one is a problem involving the advection of Leveque data [42], consists of a cone and a rectangular wave. The second is a sine wave. The Numerical solutions are computed using the one-dimensional scheme explained above. For the linear advection problem the domain is $\Omega = [-1,1]$ with periodic boundary conditions. The initial data is a cone and a rectangular wave, the rectangular wave is considered as non-smooth case, the wind velocity is considered as c = 1, In this case the flux function in eq. (1) is simply considered as $f(u) = c\ u$. The domain is partitioned into N_{elm} = 80 elements. The resulting time independent ODE is solved with the third-order SSP-RK. 400 time steps are needed for one complete revolution along the domain. Figure 4.1 shows the Leveque data after one revolution. The dotted line shows the initial data and the solid line shows the computed data after one revolution with out a limiter. The solution with out a limiter has spurious oscillations are introduced by the scheme as one can see in Figure 4.1.

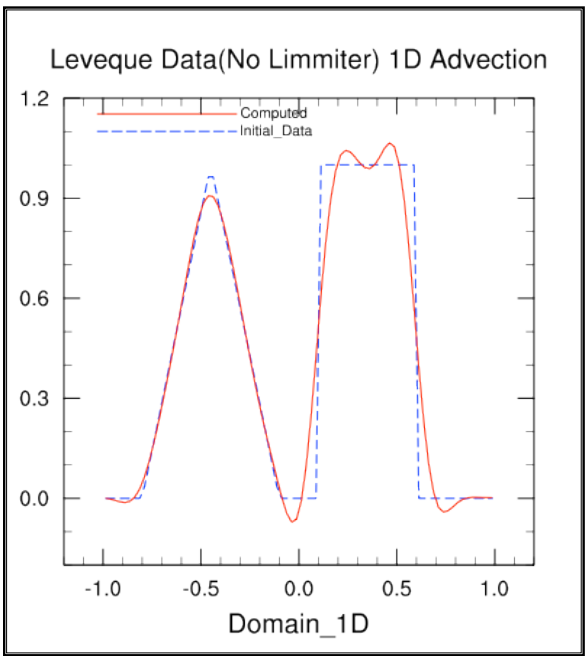

Figure 4.1: Numerical solution after one revolution of the one-dimension advection problem with the scheme considered [3]. The solution shown here is without limiting the solution. Initial data is Leveque data with computational domain $\Omega = [-1,1]$ and it consists of 80 elements.

Figure 4.2 shows the Leveque data after one revolution but this time limiting the solution using minmod limiter as explained above. One can see by comparing Figure 4.1 and Figure 4.2 the spurious oscillations are eliminated by using the limiter. And the limiter is not affecting the final solution itself and it is preserving the solution.

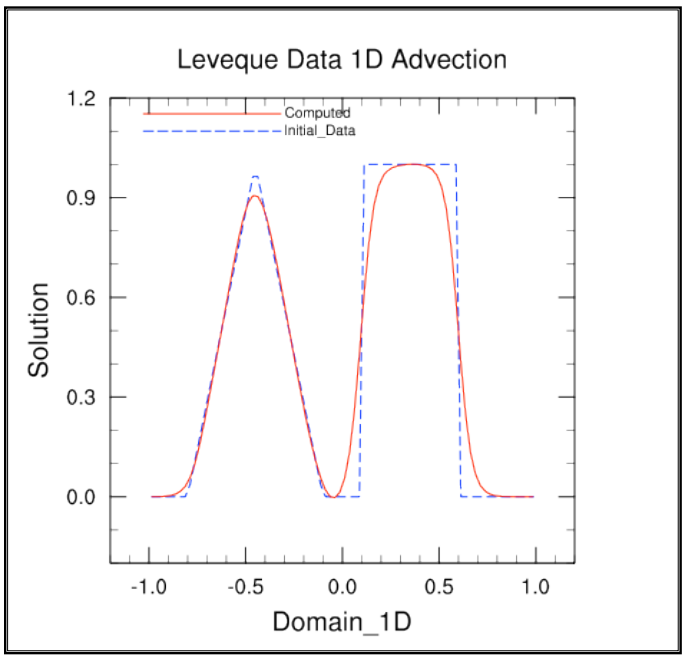

Figure 4.2: Numerical solution after one revolution of the one-dimension advection problem with the scheme considered [3]. The solution shown here is with limiting (minmod limiter) the solution. Initial data is Leveque data with computational domain Ω = [-1,1] and it consists of 80 elements.

Figure 4.3 shows the solution of sine wave after one revolution with minmod limiter. This test case is considered to demonstrate the scheme for smooth solution. The problem considered is:

$$u_t + u_x = 0; x \in [0,2\pi]$$
$$u(x,0) = sinx$$

In the Figure 4.3 the computed solution after one revolution is plotted with a solid line but it is visually indistinguishable from the initial data. So, we can say that the limiter is not affecting the computed solution; it preserves the smoothness of the solution. The solution is smooth and free from shocks.

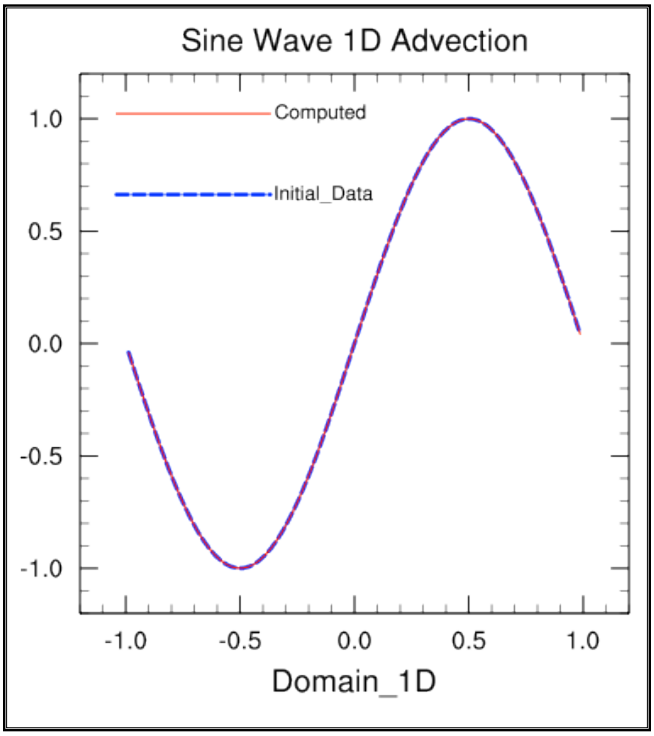

Figure 4.3: Numerical solution after one revolution of the one-dimension advection problem with the scheme considered [3]. The solution shown here is with limiting (minmod limiter) the solution. Initial data is a sine wave with computational domain Ω = [-1,1] and it consists of 80 elements.

4.2 LINEAR ACCURACY TESTS ONE-DIMENSION CASE

The accuracy of the scheme is tested on the initial boundary value problem for the linear transport equation with periodic boundary conditions.

$$u_t + u_x = 0; x \epsilon [0,2\pi]$$
$$u(x,0) = sinx$$

We calculated the L1 and L∞ errors by considering N grid points, Nelm = 40, 80, 160, 320. These errors are plotted (logarithmic scale) and are shown in Figure 4.4. The values are given Table 4.1. Order (rate) is also calculated which can be seen in Table 4.1. These values clearly validate that the solution obtained by the considered scheme is third order.

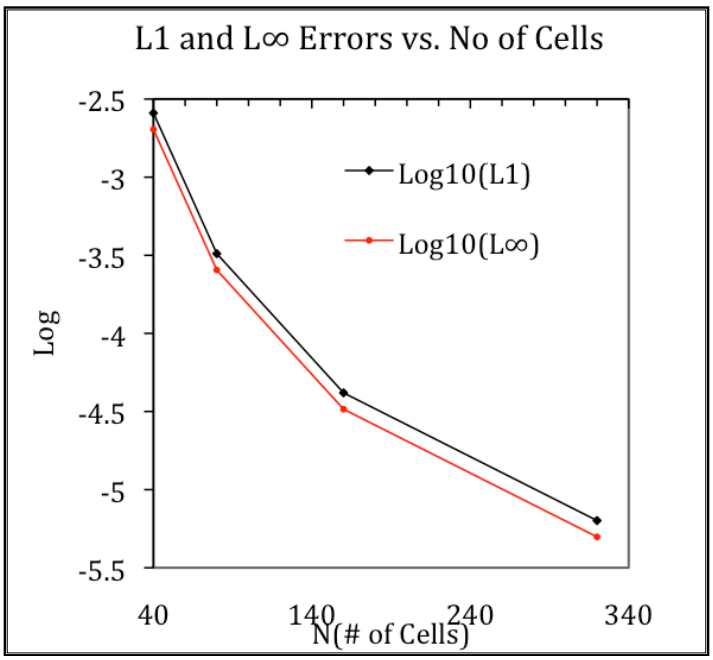

Figure 4.4: L1 and L∞ errors (Logarithmic scale), for different grid points.

Table 4.1: L1 and L∞ errors and order of the scheme (rate).

N(# of cells)	L_1 error	rate	L_∞ error	rate
40	2.57459728253895889E-003		2.02373253303633760E-003	
80	3.23984067162432496E-004	3	2.54507246700952372E-004	3
160	4.16561979646968363E-005	3	3.27189791449189471E-005	2.7
320	6.33817825783723357E-006	2.8	4.98023693862315042E-006	2.7

4.3 NUMERICAL TESTS TWO-DIMENSION CASE

We consider two standard advection tests, rotational and deformational flow problems in two-dimensions.

4.3.1 Rotational Flow

Here we considered solid body rotation test to test the scheme. Solid body rotation of Gaussian hill and a non-smooth (Leveque Data in two-dimensions) function is considered with velocity (u_x,u_y) = (-U_y,U_x), where U is given below.

Solid body rotation of Gaussian Hill

We first consider the solid body rotation of Gaussian Hill, which is a smooth function to test the scheme.

The initial condition is given by:

$$U_0(x, y) = a_0 exp[-b_0((x - x_0)^2 + (y - y_0)^2)]$$

Where a_o = 1 and b_o = 100/3.

Tests are run on the periodic domain Ω = [-1, -1] x [-1, -1] with Nelm = 40x40, with time step = 2π/2000 and number of time steps = 2000.

In the Figure 4.5 the computed solution after one rotation is plotted and is shown in the right panel (b and d) but it is visually indistinguishable from the initial data (Gaussian Hill, left panel a and c). So, we can say that the limiter is not affecting the computed solution; it preserves the smoothness of the solution and does not introduce any noises. Negligible dissipation is occurred when a smooth function is considered as initial data.

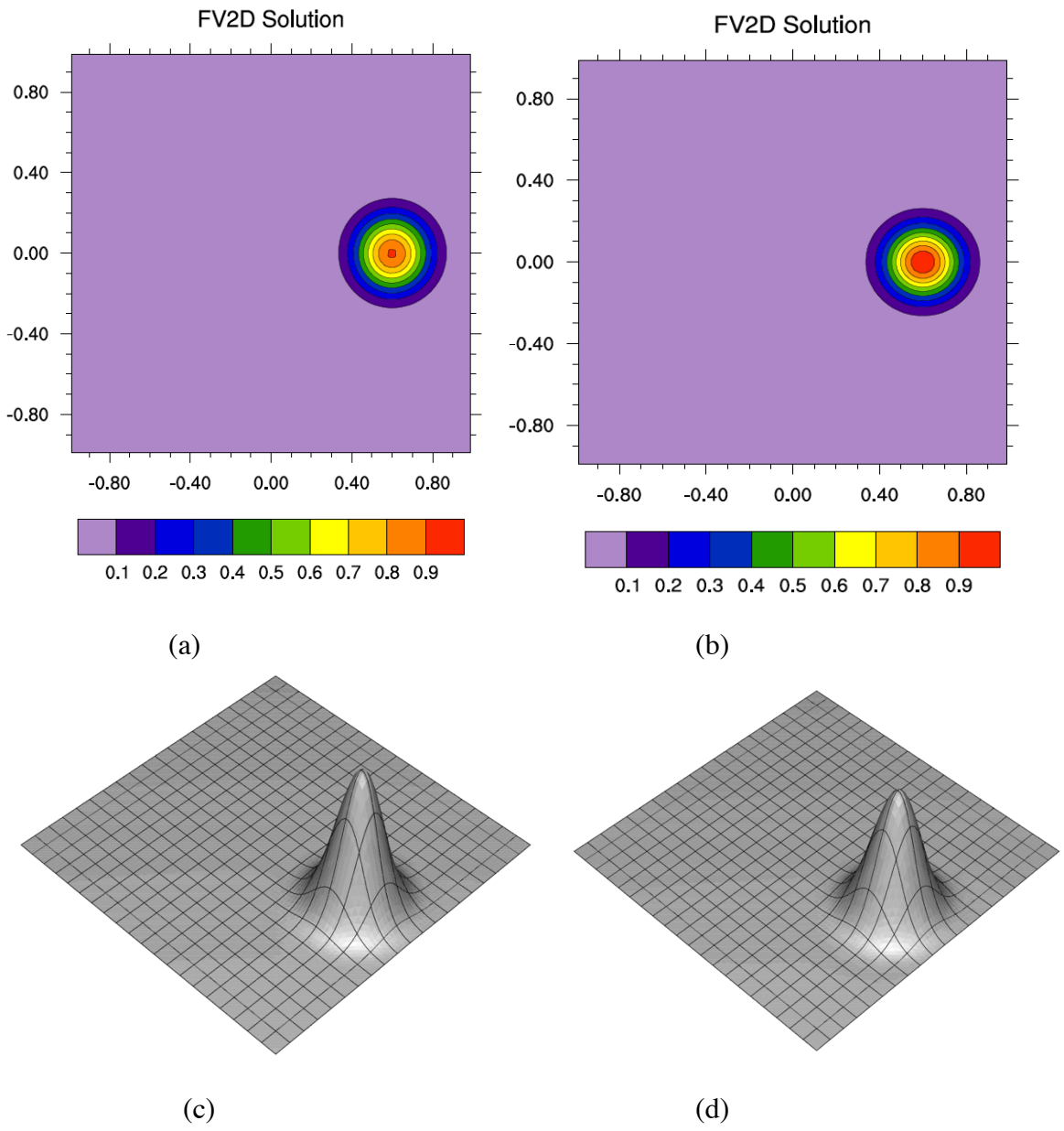

Figure 4.5: The solution shown here is with limiting (min-mod limiter) the solution in right panel (b and d) after one rotation. Initial data (a and c) is a Gaussian Hill with domain $\Omega = [-1, 1]^2$ Ne = 40x40 elements with time step = $2\pi/2000$ # of time steps = 2000.

Solid body rotation of Leveque Data (non-smooth function)

Solid body rotation test given in Leveque [42] is considered to test the scheme. This test consists of a quasi-continuous data and provides an excellent test for the monotonicity of the advecting field. The initial data is given by the following:

$$U(x,y,0) = \begin{cases} 1 & if\ .1 < x < .6\ and\ -.25 < y < .25 \\ 1 - \dfrac{r}{.35} & if\ r = \sqrt{(x+.4)^2 + y^2} < .35 \\ 0. & otherwise \end{cases}$$

The initial data is a cone, growing to a value 1 at the center and square region whose height is 1, it is plotted and can be seen in left panel of Figure 4.6 (a and c).

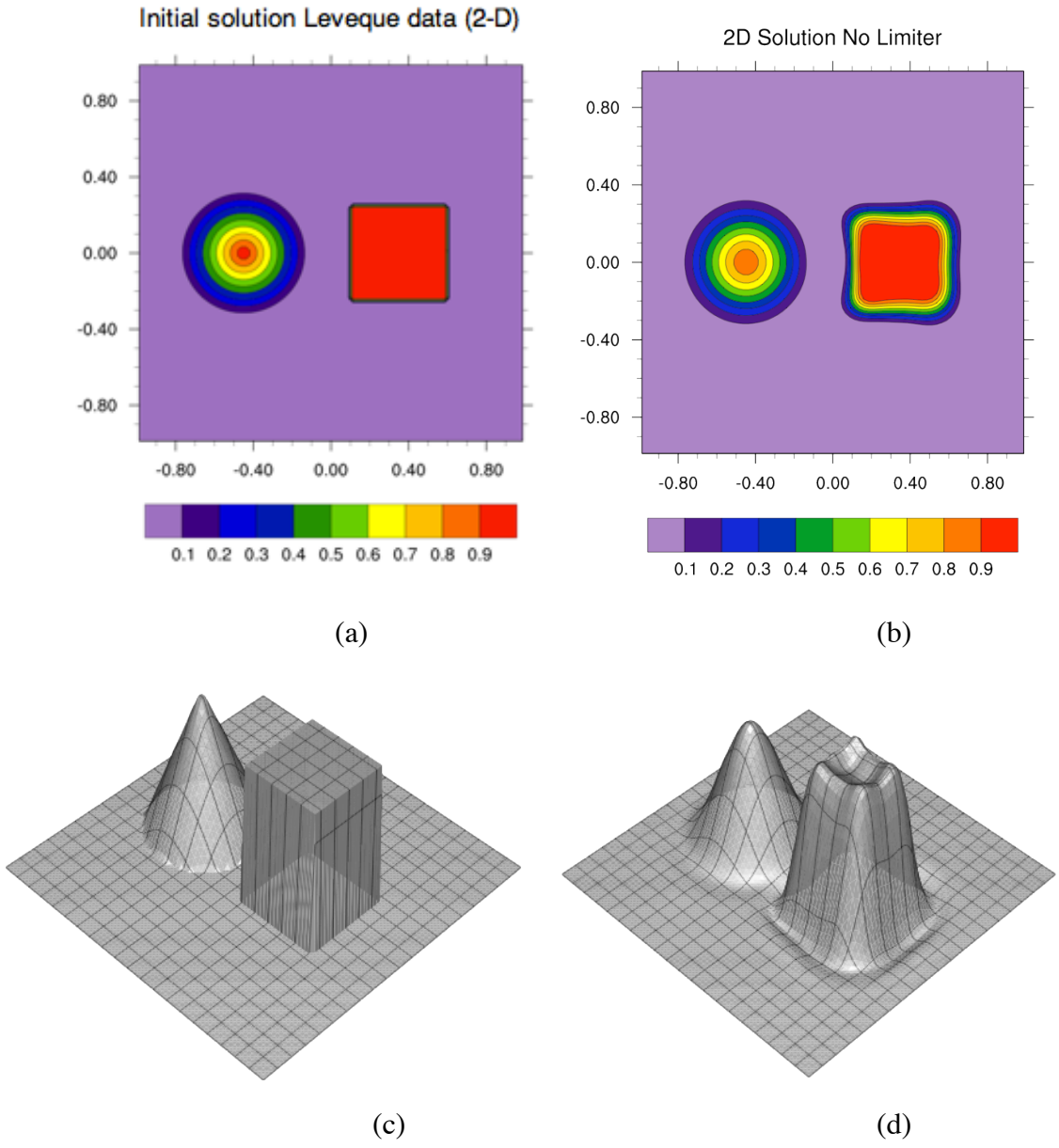

Figure 4.6: The solution shown here is without limiting the solution in right panel (b and d) after one rotation. Initial data (a and c) is a Leveque Data with computational domain Ω = [-1, 1] x [-1, 1] and it consists of 40x40 elements with time step = 2π/2000 and number of time steps = 2000.

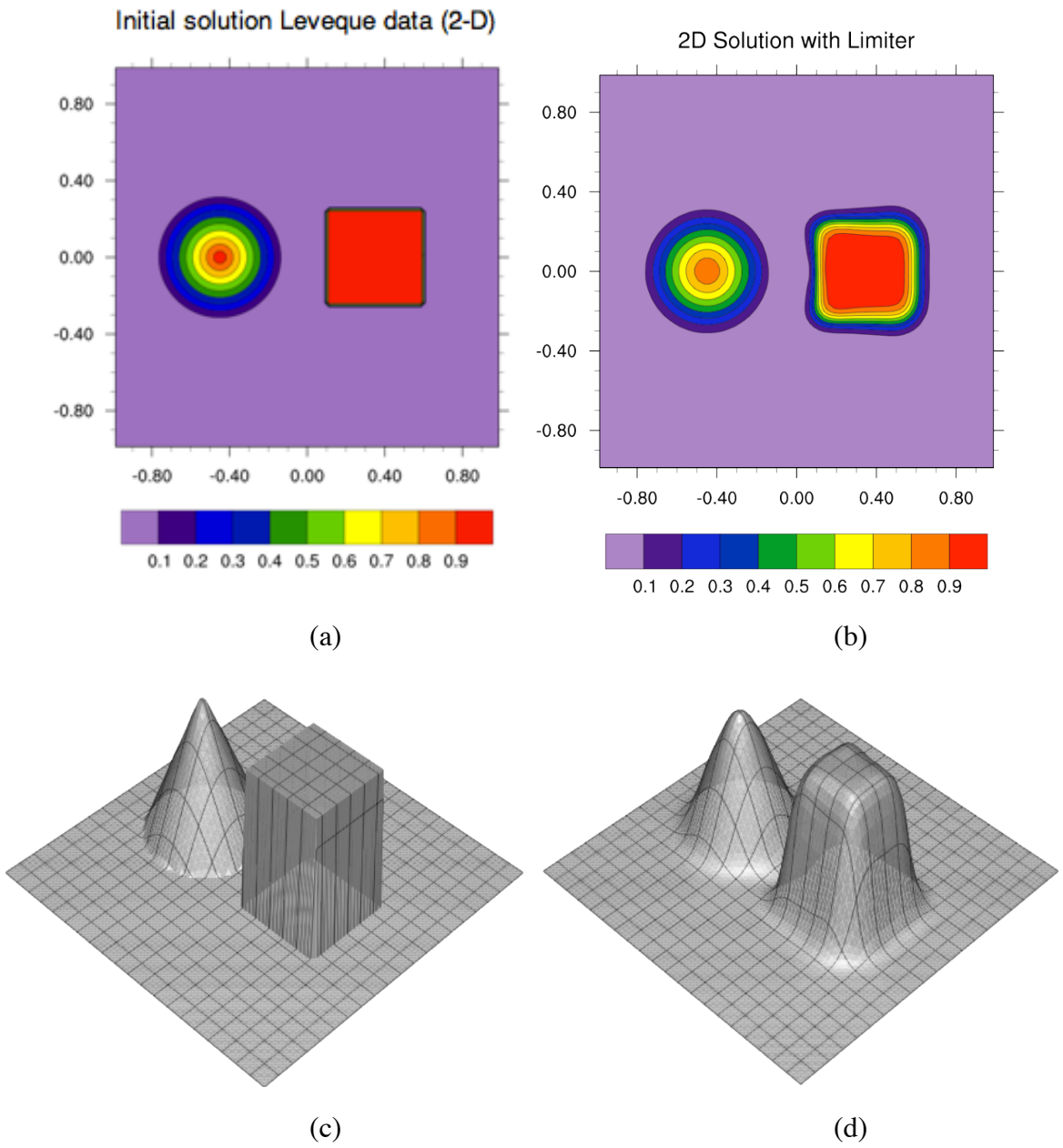

Figure 4.7: The solution shown here is with limiting (min-mod limiter) the solution in right panel (b and d) after one rotation. Initial data (a and c) is a Leveque Data with computational domain $\Omega = [-1, 1] \times [-1, 1]$ and it consists of 40x40 elements with time step = $2\pi/2000$ and number of time steps = 2000.

Figure 4.6 in the right panel (b and d) shows the result of one full solid body rotation of the function defined above for Leveque data, this solution is not limited, therefore we can see the

irregularities (spurious oscillations) at the corners (top and bottom) of the square region. Figure 4.7 in the right panel (b and d) shows the solution of one full solid body rotation with limiting the solution (min-mod limiter). The limiter removes the spurious oscillations, which are introduced by the scheme, and the solution with limiting is free from shocks and noises.

4.3.2 Deformational Flow Test

We consider a deformational test mentioned in Staniforth et al. [44], for details about this test please refer to [44]. In Figure 4.8, (a) and (c) shows the initial data considered, a cone with centre at the value 1, and, in the right panel (b) and (d), we show the solution (deformation flow with cone as initial data) with limiting after 250 time steps. Figure 4.10 (e) is taken from Staniforth et al. [44] to compare with the solution we obtained after 250 time steps. By visual inspection we can say that both Figure 4.8 (d) and (e) are almost identical.

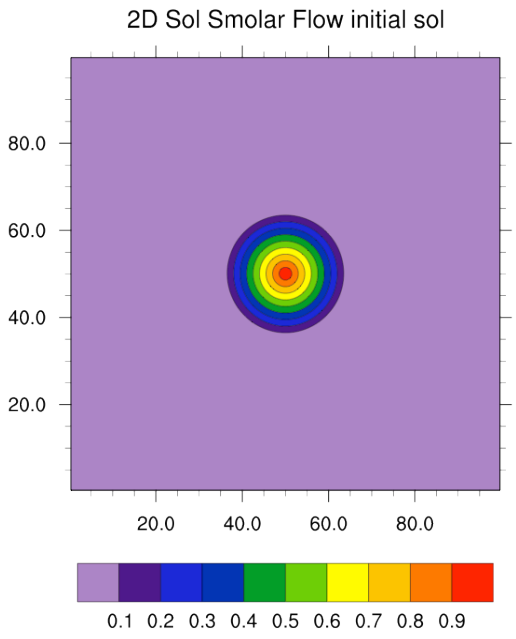

(a)

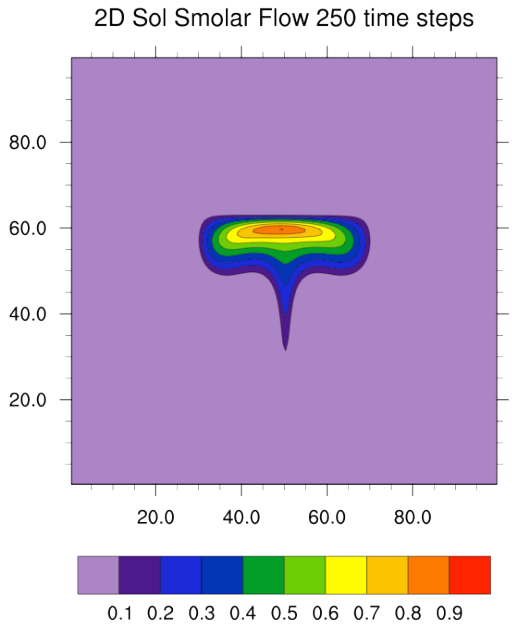

(b)

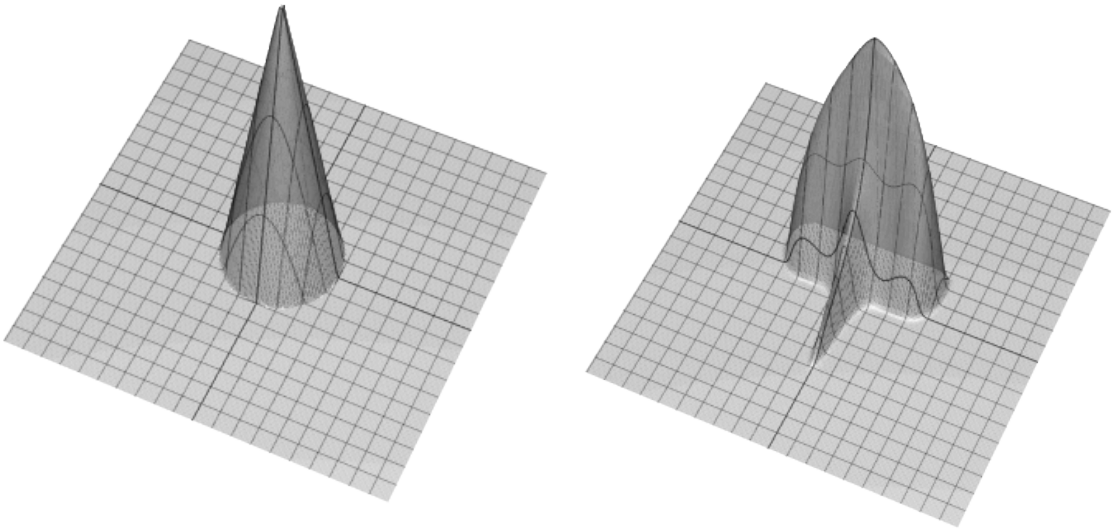

(c) (d)

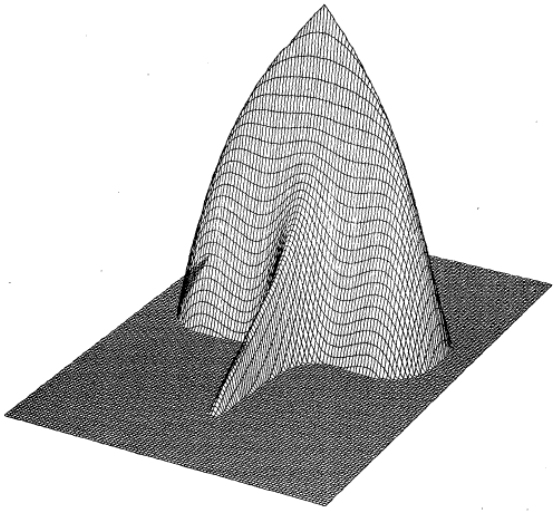

(e)

Figure 4.8: The solution shown here is with limiting (min-mod limiter) the solution in right panel (b and d) after 250 time steps. Initial data (a and c) is a cone with computational domain $\Omega = [-1, 1] \times [-1, 1]$ and it consists of 40x40 elements. The solution after 250 time steps obtained by Staniforth et al. [44] is shown in (e).

4.4 LINEAR ACCURACY TESTS TWO-DIMENSION CASE

Accuracy tests are conducted on the same problem mentioned above (Gaussian Hill), but the hill is placed at the centre. We calculated the L1 and $L\infty$ errors by considering N grid points, Nelm = 40, 80, 160. These errors are plotted (logarithmic scale) and are shown in Figure 4.9. The

values are given Table 4.2. These values clearly validate that the considered scheme is third order.

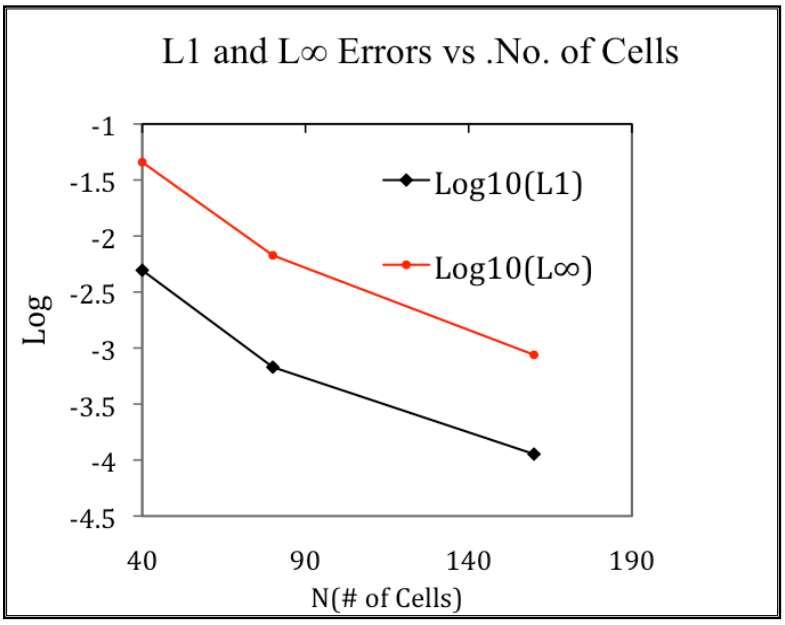

Figure 4.9: L1 and L∞ errors (Logarithmic scale), for different grid points.

Table 4.2: L1 and L∞ errors and order of the scheme (rate).

No of Cells	L1 Error	Rate	L∞ Error	Rate
40	4.95E-03		4.56E-02	
80	6.75E-04	2.87209539	6.72E-03	2.7627349
160	1.13E-04	2.579128	8.69E-04	2.95064157

Normalized global mass (integral invariant) was computed as a function of time using Eq. (135) of Williamson et al. [43], and the result is shown in Fig. 4.10. The normalized mass is conserved to the machine precision as expected and is found to be independent of the particular grid resolution used (i.e., N).

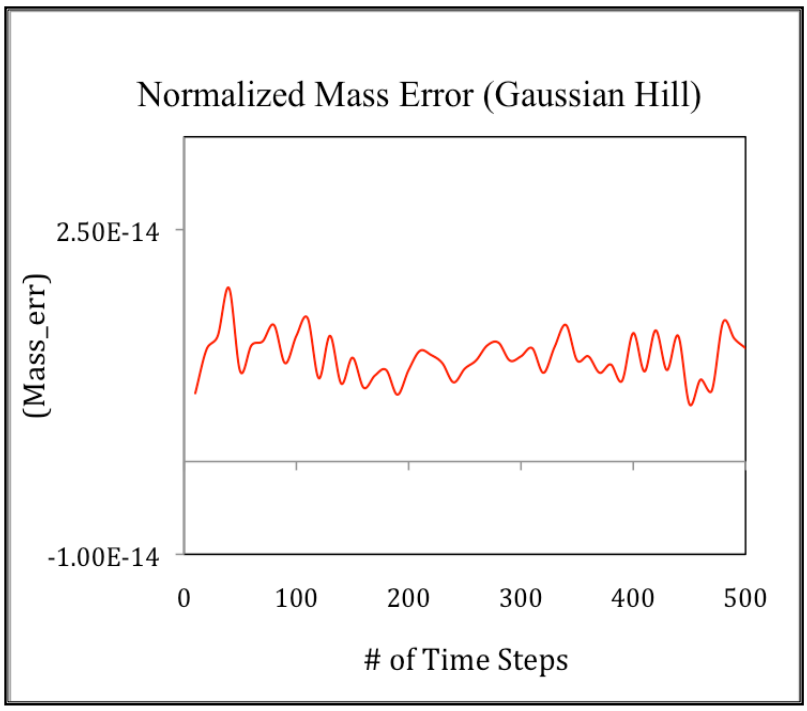

Figure 4.10: Time traces of total normalized mass error for the Gaussian Hill problem for one complete rotation. Note that the total mass is conserved to machine precision (double-precision arithmetic) and is independent of the number of elements used and polynomial degree.

Chapter 5: Future Work and Conclusions

5.1 FUTURE WORK

Future work consists of applying the scheme Kurganov et al [3] on to a cubed sphere. This involves solving of shallow water model on the cubed sphere geometry.

5.1.1 Shallow Water Model:

In modeling of the global atmospheric flows, the shallow water equations on rotating spheres are considered the primary test problems. The shallow water equations are only a first test because they don't represent the whole atmospheric system [52]. In curvilinear coordinates, the continuity and momentum equations for the shallow water system may be written as follows: (see [42], [49], [50] for further details)

$$\frac{\partial}{\partial x}\left(\sqrt{G}h\right) + \frac{\partial}{\partial x^1}\left(\sqrt{G}u^1 h\right) + \frac{\partial}{\partial x^2}\left(\sqrt{G}u^2 h\right) = 0$$

$$\frac{\partial u_1}{\partial t} + \frac{\partial}{\partial x^1}E = -\sqrt{G}u^2(f+\zeta)$$

$$\frac{\partial u_2}{\partial t} + \frac{\partial}{\partial x^2}E = -\sqrt{G}u^1(f+\zeta)$$

where

$$E = \varphi + \frac{1}{2}(u_1 u^1 + u_2 u^2)$$

$$\zeta = \frac{1}{\sqrt{G}}\left[\frac{\partial u_2}{\partial x^1} - \frac{\partial u_1}{\partial x^2}\right]$$

5.1.2 Cubed-Sphere Geometry:

Atmospheric modelers are adapting to grid systems such as cubed sphere geometry [45], to avoid singularities at the poles of the sphere, in conventional latitude-longitude grid systems. Cubed-sphere gridding takes care polar singularities due to mesh convergence in conventional global atmospheric models usually based on the latitude-longitude spherical geometry. Grid point models based on latitude-longitude grid systems also face stability restrictions in the Polar Regions and they require non-local polar filtering, which decreases the communication on a vastly parallel machine.

Sadourny [46] originally introduced the quasi-uniform spherical grid to avoid the pole problems associated with conventional spherical grids. This type of cubed sphere geometry has been recognized as commanding tool for global modeling (see [45], [47], [12]). Figure 5.1 shows the cubed sphere geometry.

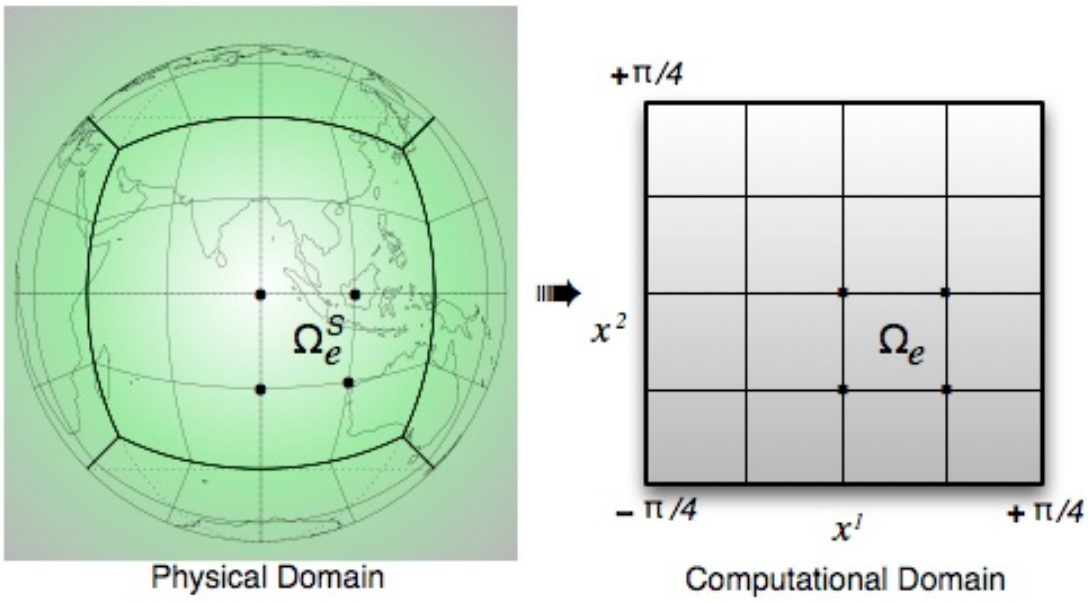

Figure 5.1 (a): Cubed Sphere geometry (Courtesy R. Nair, NCAR).

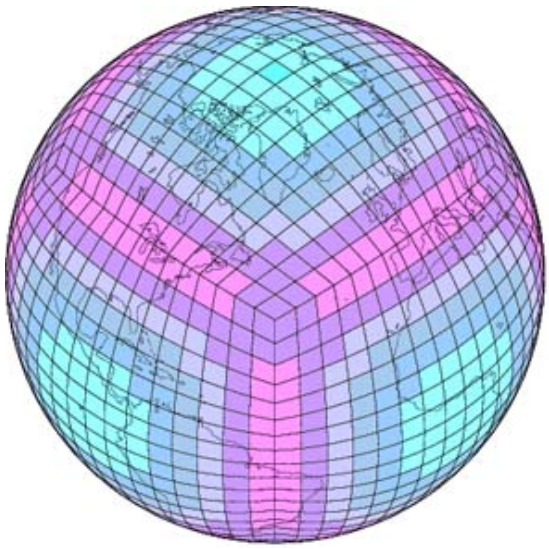

Figure 5.1 (b): The cubed-sphere grid used on each hybrid-pressure surface by the spectral element atmospheric model component of the CCSM.

A sphere is decomposed into six identical regions, obtained by a central projection of the faces of the inscribed cube onto the spherical surface. Each of the six local coordinate systems is free of singularities and employs the identical metric terms, thus creating a non-orthogonal curvilinear coordinate system on the sphere. A new level of parallelism (2D domain decomposition) is supported by Cubed sphere geometry; it is not practical within the current latitude-longitude grid implementation [48]. Here equi-angular central projection with central angles $x = x(\lambda, \theta)$, $y = y(\lambda, \theta)$ such that $x, y \in [-\pi/4, \pi/4]$ for each of the six faces, where λ and θ are the longitude and latitude coordinates, respectively is considered, it is shown in Figure 5.2. One-eighth of the cube is shown in the Figure 5.2. A point on the cube face P_1 is marked by a solid square with local Cartesian coordinates (x, y), and the corresponding point on the sphere is marked by a solid circle with absolute Cartesian coordinates (X, Y, Z). Where r is the radial distance from the center to any point (x, y) on the cube face.

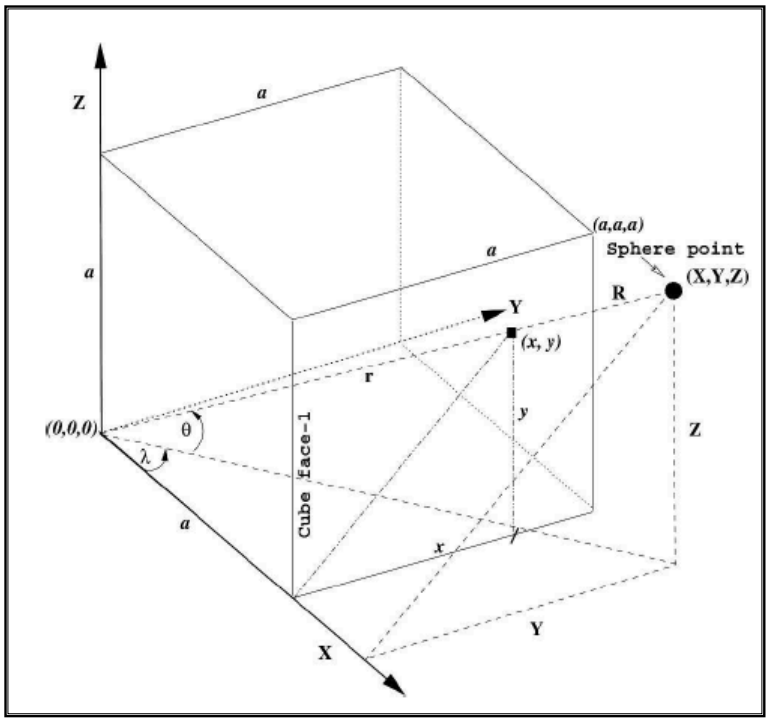

Figure 5.2: Schematic illustration of gnomonic mapping between sphere with radius R and the inscribed cube with side of length $2a$ $(a = \pi/4)$ (Courtesy R. Nair, NCAR).

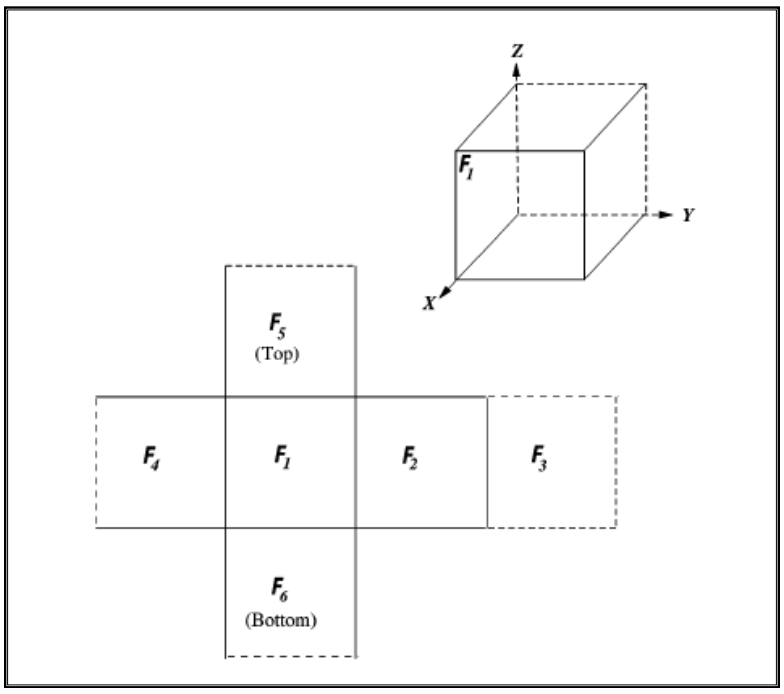

Figure 5.3: Schematic illustration of the relative positions of six cube faces (Courtesy R. Nair, NCAR).

Figure. 5.3 shows the orientation of the different cube faces and their local connectivity. Lateral faces are identified by F_n, $n = 1, \ldots 4$, whereas the top and bottom faces are F_5 and F_6 respectively. Nair et al. in [48] explained in detail the transformation laws on the six faces of the cubed-sphere. Let a_1 and a_2 be the covariant base vectors of the transformation and $v(\lambda, \theta) = (u, v)$ be the spherical velocity vector. Then the components of the covariant vectors are given by, $u_1 = v \cdot a_1$, $u_2 = v \cdot a_2$, and the corresponding contravariant vectors are related through $v = u_1 a_1 + u_2 a_2$. To transform the spherical velocity (u, v) to the cubed-sphere velocity vectors, we use the following relation:

$$A \begin{bmatrix} u^1 \\ u^2 \end{bmatrix} = \begin{bmatrix} u \\ v \end{bmatrix}$$

$$A^{-1} \begin{bmatrix} u \\ v \end{bmatrix} = \begin{bmatrix} u^1 \\ u^2 \end{bmatrix}$$

A and A^{-1} are interpreted as cube-to-sphere and sphere-to-cube transformation matrices. The metric tensor of the transformation is given by:

$$g_{ij} = A^T A$$

$$A = \begin{bmatrix} Rcos\theta \dfrac{\partial \lambda}{\partial x^1} & Rcos\theta \dfrac{\partial \lambda}{\partial x^2} \\ R\dfrac{\partial \theta}{\partial x^1} & R\dfrac{\partial \theta}{\partial x^2} \end{bmatrix}$$

$g = det(g_{ij})$, R is the radius of the sphere.

For the Finite volume formulation, each face of the cubed-sphere is partitioned into Ne x Ne rectangular non-overlapping spectral volumes. Each spectral volume is mapped onto the reference element [−1, 1] x [−1, 1], which is further divided into k x k control volumes.

Future work consists of extending the scheme for Shallow Water model on a cubed sphere, which consists of parallel implementation on supercomputer. Further incorporating this scheme in High-Order Method Modeling Environment (HOMME) framework. HOMME, a dynamical cores' component, has been integrated into the Community Atmospheric Model (CAM), which is the atmospheric component of the Community Earth System Model (CESM). CESM is a fully coupled, global climate model that provides state-of-the-art computer simulations of the Earth's past, present, and future climate states. CESM is composed of five separate models simultaneously simulating the Earth's atmosphere, ocean, land, land-ice, and sea-ice, plus one central coupler component [http://www.cesm.ucar.edu]. The CESM system can be configured a number of different ways from both a science and technical perspective. CESM supports several different resolutions and component configurations. In addition, each model component has input options to configure specific model physics and parameterizations.

HOMME provides monotonic and mass-conserving transport of multiple species, and easily couple to community physics packages such as Community Atmosphere Model (CAM) physics. Achieving these objectives will allow climate scientists to take full advantage of the petascale computing capabilities (see [51]) being deployed by NSF, and will lead to dramatic increases in climate science productivity. Next step would be to perform accuracy tests for the shallow water equations for the seven test problems as proposed in the climate simulation community:

(1) Advection of Cosine-Bell over the Pole.

(2) Global steady state nonlinear geostropic flow.

(3) Steady state zonal geostropic flow with compact support.

(4) Forced nonlinear system with a translating low.

(5) Zonal flow over isolated mountains.

(6) Rossby-Haurwitz wave.

(7) Analyzed 500 mb height and wind field initial conditions.

5.2 CONCLUSIONS

In many applications, advective processes are crucial; their treatment in the numerical modelling of the transport of trace constituents in atmospheric models is critical. Solving these equations are simple but the solutions should satisfy some constraints such as the numerical solutions should be high-order accurate, conservation of mass and energy, which is crucial for atmospheric chemistry applications. Further, these applications require solutions preserving positivity and monotonicity.

There is a need for modelers to develop grid systems and numerical algorithms that facilitate exceptional level of scalability on petascale parallel systems. The numerical algorithms that can address these challenges should have the local properties such as the high on-processor operation count and minimum parallel communication i.e. high parallel efficiency, the numerical method should also satisfy the following properties such as inherent local and global conservation, geometric flexibility, non-oscillatory advection, positivity preservation. The discretization schemes for these new generation models are based on finite-volume or spectral-element methods, and using spherical grid system such as the geodesic or cubed-sphere grid that are free from singularities.

In the present work we considered a scheme developed by Kurganov et al. [3], which can address the challenges mentioned above, which could be a potential numerical method for atmospheric modeling. Accuracy tests were performed to evaluate the scheme both in one-dimension and two-dimensions. Two standard advection tests, solid-body rotation and

deformational flow, were performed to evaluate the scheme in two dimensions. From the results presented above we can conclude that the scheme is third-order accurate, the solution is non-oscillatory and conservative. This method uses compact computational stencils, for this reason it is potential to be computationally efficient. The numerical method is coded in Fortran 90 programming language and is ready to be implemented in parallel on cubed sphere geometry.

References

[1] Nair, R. D., H. M. Tufo, 2007: Petascale atmospheric general circulation models. SciDAC 2007, June 24-28, Boston, USA. Journal of Physics: Conference Series, Vol.78

[2] Nair, R. D., H-W. Choi, and H. M. Tufo, 2009: Computational aspects of a scalable high-order discontinuous Galerkin atmospheric dynamical core. Computers & Fluids, Vol. 38, 309-319.

[3] A. Kurganov & G. Petrova (2001) "A third-order semi-discrete genuinely multidimensional central scheme for hyperbolic conservation laws and related problems"Numerische Mathematik 88, 2001, 683-729.

[4] X.-D. Liu, E. Tadmor, Third order non-oscillatory central scheme for hyperbolic conservation laws. Numerische Mathematik 79, 397–425 (1998)

[5] P. D. Lax, Weak solutions of nonlinear hyperbolic equations and their numerical computation, Comm. Pure Appl. Math. 7, 159 (1954).

[6] H. Nessyahu and E. Tadmor, Non-oscillatory central differencing for hyperbolic conservation laws, J. Comput. Phys. 87, 408 (1990).

[7] Liu X.-D., Tadmor E., Third Order Non-Oscillatory Central Scheme for Hyperbolic Conservation Laws, Numer. Math., 79, (1998), pp.397–425.

[8] Kurganov A., Tadmor E., New High-Resolution Central Schemes for Nonlinear Conservation Laws and Convection-Diffusion Equations, J. of Comp. Phys. **160**, 241–282 (2000).

[9] R. Jakob-Chien, J.J. Hack, D.L. Williamson, Spectral transform solutions to the shallow water test set, Journal of Computational Physics 119 (1995) 164–187.

[10] J. Dennis, R.D. Nair, H.M. Tufo, M. Levy, T. Voran, Development of a scalable global discontinuous Galerkin atmospheric model, International Journal of Computational Science and Engineering (2006), in press.

[11] M.O. Deville, P.F. Fischer, E.H. Mund, High-Order Methods for Incompressible Fluid Flow, Cambridge University Press, Cambridge, 2002.

[12] M. Taylor, J. Tribbia, M. Iskandarani, The spectral element method for the shallow water equations on the sphere, Journal of Computational Physics 130 (1997) 92–108.

[13] M.O. Deville, P.F. Fischer, E.H. Mund, High-Order Methods for Incompressible Fluid Flow, Cambridge University Press, Cambridge, 2002.

[14] S. Moorthi, R.W. Higgins, J.R. Bates, A global multilevel atmospheric model using a vector semi-Lagrangian finite difference scheme. Part II: Version with physics, Monthly Weather Review 123 (1995) 1523–1541.

[15] B. Cockburn, C.-W. Shu, The Runge–Kutta discontinuous Galerkin method for convection-dominated problems, Journal of Scientific Computing 16 (2001) 173–261.

[16] R.D. Nair, S.J. Thomas, R.D. Loft, A discontinuous-Galerkin global shallow water model, Monthly Weather Review 133 (2005) 876–888.

[17] M. Iskandarani, J.C. Levin, B.-J. Choi, D.B. Haidvogel, Comparison of advection schemes for high-order h–p finite element and finite volume methods, Ocean Modeling 10 (2005) 233–252.

[18] Z.J. Wang, Spectral (finite) volume method for conservation laws on unstructured grids. Basic formulation, Journal of Computational Physics 178 (2002) 210–251.

[19] Z.J.Wang, Y. Liu, Spectral (finite) volume method for conservation laws on unstructured grids: Extension to two-dimensional scalar equation, Journal of Computational Physics 179 (2002) 665–697.

[20] B.-J. Choi, M. Iskandarani, J. Levin, D.B. Haidvogel, A spectral finite-volume method for the shallow water equations, Monthly Weather Review 132 (2004) 1777–1791.

[21] Vani Cheruvu, Ramachandran D. Nair, Henry M. Tufo, A spectral finite volume transport scheme on the cubed-sphere, Applied Numerical Mathematics archive Volume 57 Issue 9, September, 2007.

[22] G.E. Karniadakis, S.J. Sherwin, Spectral/hp Element Methods for CFD, Oxford University Press, Oxford, 1999.

[23] Godunov, S. K. (1959), "A Difference Scheme for Numerical Solution of Discontinuous Solution of Hydrodynamic Equations", Math. Sbornik, 47, 271–306, translated US Joint Publ. Res. Service, JPRS 7226, 1969.

[24] Hirsch, C. (1990), Numerical Computation of Internal and External Flows, vol 2, Wiley.

[25] K.O. Friedrichs, Symmetric hyperbolic linear differential equations.Comm.Pure Appl. Math. 7 345–392 (1954)

[26] F. Bianco, G. Puppo, G. Russo, High order central schemes for hyperbolic systems of conservation laws. SIAM J. Sci. Comp.

[27] D. Levy, G. Puppo, G. Russo, Central WENO schemes for hyperbolic systems of conservation laws. Math. Model. and Numer. Anal. 33:3, 547–571 (1999)

[28] P. Arminjon, M.-C. Viallon, G´en´eralisation du sch´ema de Nessyahu-Tadmor pour une equation hyperbolique `a deux dimensions d'espace. C.R. Acad. Sci. Paris, t. 320, s´erie I (1995), pp. 85–88

[29] G.-S. Jiang, E. Tadmor, Non-oscillatory central schemes for multidimensional hyperbolic conservation laws. SIAM J. Sci. Comp. 19, 1892–1917 (1998)

[30] D. Levy,G. Puppo, G. Russo, Athird order centralWENOscheme for 2D conservation laws. Applied Numerical Mathematics 33 (2000) 415–421

[31] D. Levy, G. Puppo, G. Russo, Compact central WENO schemes for multidimensional conservation laws. SIAM J. Sci. Comput 2000.

[32] A. Harten, High resolution schemes for hyperbolic conservation laws. J. of Comp Phys. 49, 357–393 (1983).

[33] A. Harten, B. Engquist, S. Osher, S.R. Chakravarthy, Uniformly high order accurate essentially non-oscillatory schemes III. J. of Comp. Phys. 71 231–303 (1987).

[34] A. Kurganov, Conservation laws: stability of numerical approximations and nonlinear regularization. Ph.D. Thesis, Tel-Aviv University, Israel (1997).

[35] B. van Leer, Towards the ultimate conservative difference scheme, V. A second order sequel to Godunov's method. J. of Comp. Phys. 32, 101–136 (1979).

[36] S. Osher, E. Tadmor, On the convergence of difference approximations to scalar conservation laws. Math. Comp. 50 19–51 (1988).

[37] C.-W. Shu, S. Osher, Efficient implementation of essentially non-oscillatory shock capturing schemes. J. Comp. Phys. 77, 439–471 (1988).

[38] X.-D. Liu, S. Osher, T. Chan, Weighted essentially non-oscillatory schemes. J. of Comp. Phys. 115, 200–212 (1994).

[39] G.-S. Jiang, C.-W. Shu, Efficient implementation of weighted ENO schemes. J. of Comp. Phys. 126, 202–228(1996).

[40] S. Gottlieb, C.-W. Shu, E. Tadmor, Strong stability preserving high-order time discretization methods, SIAM Review 43 (2001) 89–112.

[41] Cockburn, B., and C. W. Shu, 1989: TVB Runge–Kutta local projection discontinuous Galerkin method for conservation laws. II: General framework. Math. Comput., 52, 411 435.

[42] Randall J. LeVeque 2004, Finite Volume Methods for Hyperbolic Problems, Cambridge University Press.

[43] Williamson, D. L., J. B. Drake, J. Hack, R. Jacob, and P. N. Swartztrauber, 1992: A standard test set for numerical approximations to the shallow water equations in spherical geometry. J. Comput. Phys., 102, 211–224.

[44] A. Staniforth, J. Cot´e, J. Pudickiewicz, Comments on "Smolarkiewicz's deformational flow", Mon. Wea. Rev. 115 (1987) 894–900.

[45] C. Ronchi, R. Iacono, P.S. Paolucci, The "Cubed sphere": A new method for the solution of partial differential equations in spherical geometry. Journal of Computational Physics 124 (1996) 93–114.

[46] Sadourny, R., 1972: Conservative finite-difference approximations of the primitive equations on quasi-uniform spherical grids. Mon. Wea. Rev., 100, 136–144.

[47] McGregor, J. L., 1996: Semi-Lagrangian advection on a conformal cubic grid. Mon. Wea. Rev., 124, 1311–1322.

[48] R.D. Nair, S.J. Thomas, R.D. Loft, A discontinuous Galerkin transport scheme on the cubed-sphere, Monthly Weather Review 133 (2005) 814–828.

[49] Arakawa, A., and V. R. Lamb, 1981: A potential enstrophy and energy conserving scheme for the shallow-water equations. Mon. Wea. Rev., 109, 18–36.

[50] Rancˇic´, M. R., J. Purser, and F. Mesinger, 1996: A global-shallow water model using an expanded spherical cube. Quart. J. Roy. Meteor. Soc., 122, 959–982.

[51] R. D. Nair and H. M. Tufo, 2007: Petascale Atmospheric General Circulation Models. Journal of Physics: Conference Series 78 (2007) 012078.

[52] Taylor, M., Tribbia, J., & Iskandarani, M. (1997). The Spectra Element Method for the Shallow WaterEquations on the Sphere. *Journal of Computational Phys. , 130*, 92-108.

Vita

Kiran K Katta was born on January 16, 1985 in Madhira, India, he is the eldest child of Nageshwara Rao Katta and Padmavathi Katta and has lived in Hyderabad, India since the age of 5 until he came to El Paso for his Masters. He completed his high-school education at Narayana Jr College, Hyderabad, India in 2002 and was awarded Bachelors of Engineering (Mechanical Engineering) by Osmania University in May 2006. He was awarded Masters of Science (Mechanical Engineering) by University of Texas at El Paso (UTEP) in Dec 2008. While at UTEP, Kiran Katta has worked as a graduate research and teaching assistant. He also worked for Cummins Inc as CPE Engineer for a period of one year (Apr 2008 – Apr 2009). He was given an opportunity as an Intern (SIParCS summer - 2010) at National Center for Atmospheric Center (NCAR). Presently he is pursuing his Doctoral Studies (started Aug 2009) in "Program in Computational Science" (CPS) at UTEP.

Permanent Address: D-97 Madhuranagar,

Hyderabad, AP, India, 500038.

This thesis was typed by Kiran Kumar Katta.